Quaternary Science Reviews 284 (2022) 107497

Contents lists available at ScienceDirect

Quaternary Science Reviews

journal homepage: www.elsevier.com/locate/quascirev

High-resolution calibration of seismically-induced lacustrine deposits with historical earthquake data in the Eastern Alps (Carinthia, Austria)

Christoph Daxer [a, *], Marcel Ortler [a], Stefano C. Fabbri [b], Michael Hilbe [b], Irka Hajdas [c], Nathalie Dubois [d], Thomas Piechl [e], Christa Hammerl [f], Michael Strasser [a], Jasper Moernaut [a]

[a] Institute of Geology, University of Innsbruck, Austria
[b] Institute of Geological Sciences and Oeschger Centre of Climate Change Research, University of Bern, Switzerland
[c] Laboratory of Ion Beam Physics, ETH Zurich, Switzerland
[d] Surface Waters-Research and Management, Eawag, Swiss Federal Institute of Aquatic Science and Technology, Dübendorf, Switzerland
[e] Amt der Kärntner Landesregierung, Klagenfurt, Austria
[f] ZAMG – Zentralanstalt für Meteorologie und Geodynamik, Vienna, Austria

ARTICLE INFO

Article history:
Received 17 May 2021
Received in revised form
24 March 2022
Accepted 26 March 2022
Available online 7 April 2022

Handling Editor: Yan Zhao

Keywords:
Paleoseismology
Lake sediments
Mass-transport deposits
Turbidites
Alps

ABSTRACT

Lake sediments are increasingly used to reconstruct recurrence intervals of large earthquakes - a prerequisite for the establishment of accurate seismic hazard models - because they can record strong seismic shaking as mass-transport deposits (MTDs), turbidites or sediment deformations and often reach back several thousands of years. To derive quantitative information on paleo-earthquake size, the sedimentary imprints need to be thoroughly calibrated with independent information on seismic shaking strength. A few calibration studies proposed scaling relationships between the shaking strength of historical earthquakes and the type and size of lacustrine sedimentary imprints. Due to incomprehensive lacustrine mapping or an insufficient record of documented earthquakes, however, rigorous testing of these scaling relationships is lacking. Here, we study the sedimentary infill of the past ~800 years in Wörthersee and Millstättersee, two large lakes in the Eastern Alps (Carinthia, Austria). These lakes have experienced five well-documented historical earthquakes with local seismic intensities ranging from V – IX (EMS-98 scale). We trace the sedimentary signatures (MTDs and turbidites) of these earthquakes based on a vast dataset of multibeam bathymetry, reflection seismic profiles and numerous precisely dated sediment cores. Seismic intensities as low as V½ are recorded as turbidites originating from deltaic slopes, while hemipelagic slopes can fail from intensities of VI onwards. In Wörthersee, earthquake-recording thresholds are highly dependent on the specific core locations due to local variations in slope characteristics (composition, length, and gradient) and transport distance to the core site. This highlights the potential for establishing multi-threshold paleoseismic records based on multiple coring sites in a single basin. In both lakes, exponential size-scaling relationships are inferred between seismic intensity and i) number or volume of mass-transport deposits and ii) the cumulative thickness of turbidites. Moreover, the relative turbidite presence increases linearly with seismic intensity, confirming the results from a previous study in Chilean lakes. Application of the obtained size-scaling relationships on the first major earthquake documented for Austria (1201 CE) suggests a magnitude of ~6.4 and an epicentre close to Millstätter See. This demonstrates that lake paleoseismology is a powerful tool to obtain quantitative information on the seismic intensity distribution of paleo-earthquakes.

1. Introduction

In intraplate settings characterized by slow deformation rates and migrating, episodic and spatially clustered seismicity, recurrence intervals of strong earthquakes (moment magnitude $M_w > 6$) typically exceed the short time span of instrumental and historical

* Corresponding author. Innrain 52f, 6020, Innsbruck, Austria.
E-mail address: christoph.daxer@uibk.ac.at (C. Daxer).

https://doi.org/10.1016/j.quascirev.2022.107497

records (Stein et al., 2017). To constrain average recurrence intervals, recurrence patterns and maximum possible magnitudes of strong earthquakes needed to assess seismic hazards in these regions, the geoscientific community increasingly resorts to lakes as event archives. Lacustrine sediments can record strong seismic shaking as mass-transport deposits (MTDs), turbidites or sediment deformation structures and can form long, continuous and sensitive paleoseismic archives (e.g. Strasser et al., 2013; Kremer et al., 2017; Moernaut, 2020; and key references therein). Because an earthquake record which fails to provide information on seismic shaking strength or earthquake magnitude is of limited use, the sedimentary imprints need to be thoroughly calibrated with independent information on such earthquake parameters. The main approach consists of tracking the imprint of well-documented recent and historical earthquakes and applying this information on the prehistorical sediment record (Hibsch et al., 1997; Kremer et al., 2017; Moernaut et al., 2014). Other strategies include numerical modelling of deformation structures (Lu et al., 2020) or the evaluation of subaqueous slope stability conditions (Strasser et al., 2011). As lake systems provide a wide range of lithologies and morphologies and are located in different seismotectonic settings, site-specific approaches to identify and calibrate the sedimentary imprints are necessary. For example, large (>1 km^2) and deep (>30 m) lakes typically present paleoseismic evidence related to subaqueous mass wasting (MTDs and turbidites; e.g. Schnellmann et al., 2002; Waldmann et al., 2008; Praet et al., 2017). Multiple event deposits on a single stratigraphic level suggest synchronicity of several slope failures, which has proven to be a strong argument for seismic triggering ("synchronicity criterion"; Schnellmann et al., 2002). Small and shallow lakes often exhibit more subtle earthquake signatures such as i) in-situ sediment deformation structures (Monecke et al., 2006; Oswald et al., 2021b), ii) seiche-related resuspension of coastal sediments (Avşar et al., 2014) and iii) post-seismic changes in lake sediment geochemistry (Archer et al., 2019). To produce a specific imprint, seismic intensity must overcome a certain threshold: deltas can fail from intensities of V–V½ onwards (Moernaut et al., 2014; Van Daele et al., 2019), but may also be subject to spontaneous failure without external seismic trigger (Girardclos et al., 2007). Hemipelagic slopes are less sensitive to seismic shaking and generally fail at seismic intensities ≥ VI (Moernaut et al., 2014; Monecke et al., 2004; Van Daele et al., 2015; Wilhelm et al., 2016). Several other site-specific factors such as sedimentation rate might affect these threshold values (Wilhelm et al., 2016). In specific locations, such as in large Chilean piedmont lakes and Alaskan proglacial lakes, it is inferred that also the relative presence and size of turbidites scales to seismic intensity and can thus be used to obtain information on seismic shaking strength of paleo-earthquakes (Moernaut et al., 2014; Molenaar et al., 2021; Van Daele et al., 2019; 2015). Such quantitative data can be used to better constrain rupture location and extent (Howarth et al., 2016, 2021; Wils et al., 2020) and provides insights into recurrence patterns of different earthquake sizes (Moernaut et al., 2018), which are crucial input data for developing robust seismic hazard models.

Besides the Chilean and Alaskan case studies, no studies have evaluated whether the size of the lacustrine imprint can be used as a proxy for shaking strength. This was proposed for e.g. the volume of mass movements in terrestrial settings (Silva et al., 2015). Such size-scaling evaluation for the lacustrine realm requires i) a comprehensive basin-wide mapping and accurate dating of earthquake imprints and ii) multiple well-documented historical earthquakes that are sufficiently spaced in time and exhibited different intensities at the studied lake. Here, we study large lakes situated in the Eastern European Alps. Given the multiple basins in each lake that allow application of the synchronicity criterion, the presence of annually laminated sediments, and a well-known history of several strong earthquakes with varying intensities at the lake sites, these lakes constitute exceptional sites to meet above mentioned criteria and advance lacustrine paleoseismology in intraplate settings.

2. Regional setting

2.1. Seismotectonic setting & historical earthquakes

The studied lakes Wörthersee and Millstätter See are situated in Carinthia (Austria), close to the border to Slovenia and Italy (Fig. 1). The seismotectonic regime is governed by ongoing plate convergence of ~2–3 mm/yr related to the northward indentation and anticlockwise rotation of the Adriatic microplate (Sánchez et al., 2018). This process has been active since the Late Oligocene/Middle Miocene and caused the eastward extrusion of decoupled crustal blocks that originate from the Adriatic microplate (also called "Austroalpine units"), which was accommodated by low angle normal faults and major strike-slip fault systems (Ratschbacher et al., 1991) that border the study site (Fig. 1a): The Katschberg fault and the Mölltal fault in the west, the Mur-Mürz fault system in the north, the Lavanttal fault zone in the east and the Periadriatic fault system in the south. Seismic activity along these faults indicates that the lateral extrusion is still ongoing, but moderate to strong earthquakes are rare (Fig. 1a; Reinecker and Lenhardt, 1999; Eder and Neubauer, 2000). The Periadriatic fault system merges with the seismically active Sava fault system in the east and separates the Eastern Alps from the Southern Alps (e.g Kastelic et al., 2008). The Italian part of the Southern Alps (Friuli area) is characterized by south-directed thrusts (Castellarin and Cantelli, 2000). Towards the East, in the Dinaric system, dextral NW-SE striking faults are predominant (e.g. the Idrija fault, Fig. 1; Moulin et al., 2016). Although the major tectonic activity caused by the progressive motion of the Adriatic microplate dates to the Miocene and has shifted towards the Mediterranean (Brückl et al., 2010), the border region of Italy, Slovenia and Austria still is one of the tectonically most active part of the Alps (Priolo et al., 2005).

The earliest damaging earthquake reported in the studied region happened on May 4, 1201 Common Era (CE). Due to the sparse availability of historical reports, the epicentral location and intensity (I_0) are unclear. In older literature (e.g. Toperczer and Trapp, 1950; Alexandre, 1990), an epicentre near Murau (1201b CE in Fig. 1a) and I_0 of IX (Medvedev-Sponheuer-Karnik scale, MSK) are assumed. Upon a critical review of historical sources, Hammerl (1995, 2008) proposed an epicentre close to the Katschberg region in Carinthia (*1201a CE* in Fig. 1a). On January 25, 1348 CE, the strongest reported earthquake in the Alps hit the study area with a reconstructed moment magnitude (M_w) of ~7 and an I_0 of IX-X (Mercalli-Cancani-Sieberg scale, MCS; Guidoboni et al., 2019). The epicentre location is still debated, ranging from the vicinity of Villach (therefore also called "Villach-Earthquake"; e.g. Guidoboni and Comastri, 2005a) to the Friuli region in Italy (1348b CE in Fig. 1a; e.g. Hammerl, 1994). Nevertheless, the local macroseismic intensities (I_L) in the study area are well constrained (~IX-X near Villach and VIII-IX near Wörthersee and Millstätter See, Fig. 1b; Stucchi et al., 2013). On March 26, 1511 CE, the study area was affected by a strong earthquake (M_w ~6.9, I_0 IX) with an epicentre close to the Slovenian-Italian border. Reports on damage in Carinthia are sparse, but some sources describe heavy damage in Villach, hinting at I_L ~ VII-VIII (Fig. 1c; Camassi et al., 2011 and references therein). Another devastating earthquake occurred on December 04, 1690 CE (M_w ~6.5, I_0 VIII½). Based on the distribution of intensity data points (IDPs), the epicentral area of this earthquake was estimated to a location about 5 km northwest of Villach

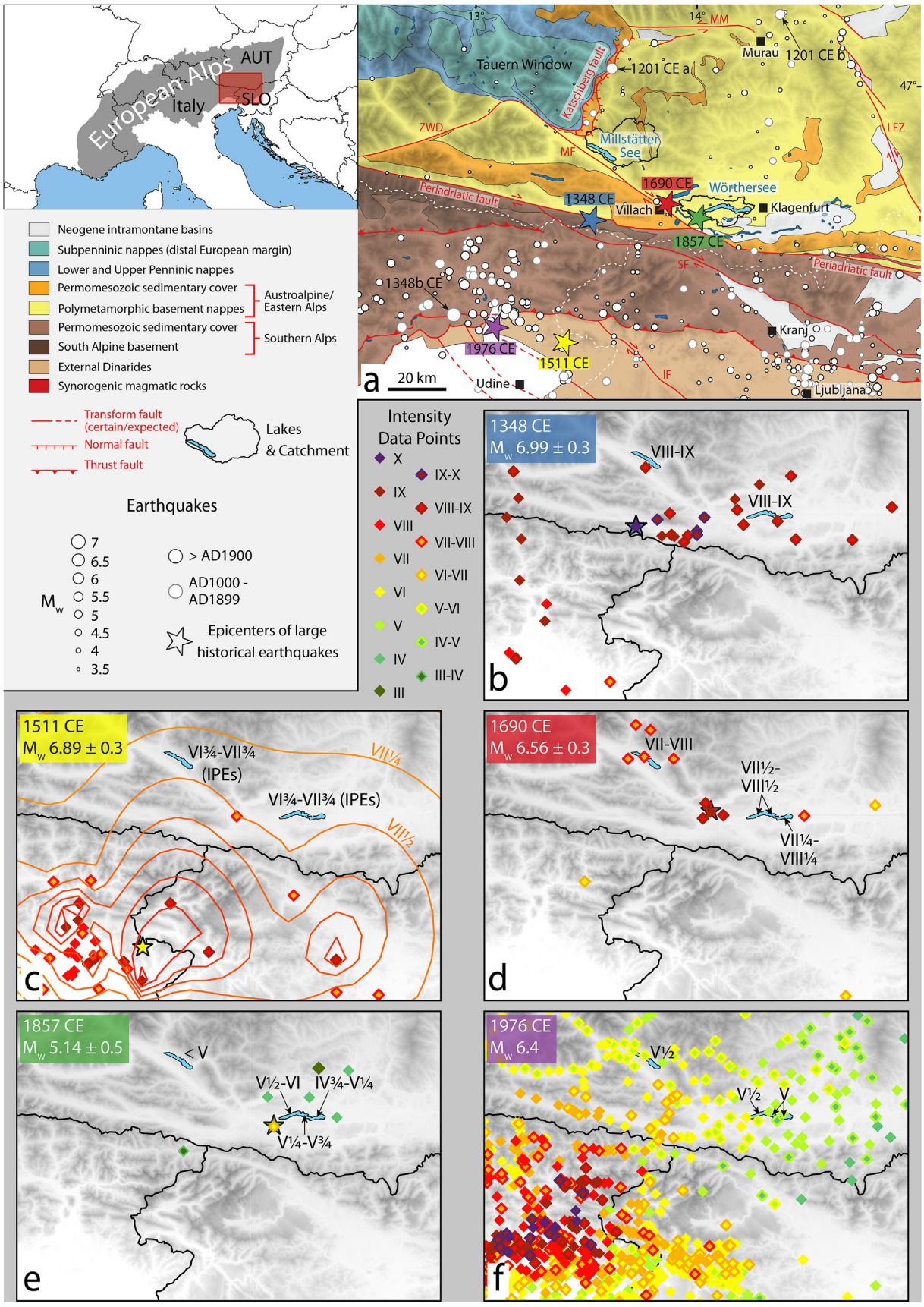

Fig. 1. **(a)** General seismotectonic setting of the study area (simplified from Reinecker and Lenhardt, 1999; Schmid et al., 2004; Reiter et al., 2018). IF: Idrija fault, LFZ: Lavanttal fault zone, MF: Mölltal fault, MM: Mur-Mürz fault, SF: Sava fault, ZWD: Zwischenbergen-Wöllatratten-Drau fault. Earthquake epicentres and magnitudes were compiled from SHEEC 1000–1899 (Stucchi et al., 2013), SHEEC 1900–2006 (Grünthal et al., 2013) and the Austrian earthquake catalogue (ZAMG, 2021). For the 1201 CE earthquake, two possible

(Fig. 1d; Guidoboni et al., 2019). The earthquake led to severe building damage in Millstatt (VII-VIII), Villach (IX) and Klagenfurt (VII-VIII) and caused several fatalities (Ambraseys, 1976; Delbrück, 2010). On December 25, 1857 CE, a smaller earthquake caused the collapse of a building and damaged houses about 3 km southwest of Velden am Wörthersee (I_0 VI-VII; M_w ~5.1 according to Stucchi et al., 2013; M_L ~4.6 according to ZAMG, 2021). In Klagenfurt, this earthquake only caused minor shaking (I_L ~ IV; Fig. 1e; see supplementary data 2). The most recent devastating earthquake in the broader region occurred on May 6, 1976 CE in Friuli, ~70 km south of the study area. Together with two earthquakes on September 15, 1976 (M_w 5.9 and 6.1), this event (M_w of 6.4, I_0 X) caused almost 1000 fatalities, but only led to minor damage in the study area (I_L ~ V-VI; Fig. 1f; Tertulliani et al., 2018).

2.2. Setting of studied lakes

Wörthersee (46°38′ N, 14°9′ E; 439 m a.s.l.) and Millstätter See (46°48′ N, 13°35' E; 588 m a.s.l.; *See* = German for lake) are lakes embedded into overdeepened troughs that were successively carved along pre-existing strike-slip faults and their auxiliary faults during Pleistocene glaciations (Anderle, 1977; Kahler, 1962; Pistotnik et al., 1980; Reitner, 2005). After the onset of westward retreat of the Drau glacier at 18–19 ka BP (Reitner, 2007; Schuster et al., 2006), dead ice bodies hampered sedimentation in the valleys now occupied by the lakes (Reitner et al., 2005). Their ice-free surroundings quickly filled with fluvioglacial sediments in the form of Kame terraces and alluvial fans, damming the lake outflow after melting of the ice.

2.2.1. Wörthersee

Wörthersee is the largest lake in Carinthia, covering 19.4 km^2 and draining a catchment area of 162 km^2. It is located within metamorphic crystalline units (mainly phyllites and mica-schists; Homann, 1962) and separated into three main basins by bedrock and/or moraine ridges (Fig. 2a): i) the western basin (up to ~84 m deep), stretching from Velden to Pörtschach; ii) the middle basin (~40 m), which is subdivided into 3 subbasins, stretching from Pörtschach to Reifnitz; and iii) the eastern basin (~72 m), subdivided into two subbasins, stretching from Reifnitz to Klagenfurt. The main inflow, the Reifnitzbach ("Bach" = German for small river), has only a small mean discharge of 0.63 m^3/s (Kärntner Institut für Seenforschung, 1992) and enters the lake in the eastern basin. It drains Keutschacher See, a small lake situated ~2.5 km upstream. Most other inflows are small streamlets entering the lake in the western basin. The lakes' outflow in the east is a (nowadays) artificially regulated channel, the Glanfurt, situated in the east. With the artificial deepening and engineering of this outflow in 1770, the lakes' water level dropped at least 1–2 m. Wörthersee is an intermittently meromictic/oligomictic lake. Generally, mixing only occurs to depths of 50–60 m in spring and autumn. Occasionally, however, the water column mixes down to the lake bottom (Reichmann et al., 2014). Therefore, the deepest parts of the western and eastern basins mostly lack oxygen, whereas the middle basin is permanently oxygenated. Since at least the 1960s, the deepest waters of Wörthersee were subject to enhanced oxygen depletion due to increased nutrient influx, accompanied by a lowering of water transparency (Kärntner Institut für Seenforschung, 1992). Especially in summertime, white turbid waters caused by authigenic calcite precipitation are common. The calcite accumulates in calm near-shore areas, leading to characteristic white lake marl banks. Most of the littoral zone (77%) is in a non-natural state due to shoreline reinforcement and the building of houses and jetties (Schulz et al., 2008). These construction works caused several coastal slope failures, especially in the western basin. Most MTDs visible in today's bathymetry, however, resulted from seismic shaking during the 1348 CE earthquake (Daxer et al., 2020).

2.2.2. Millstätter See

Millstätter See is the deepest (137 m) and second largest lake in Carinthia, covering an area of 13.3 km^2. The main inflow, the Riegerbach river (average discharge 3.2 m^3/s; Kärntner Institut für Seenforschung, 1992), enters the lake in the south-east (Fig. 2c). It drains 188 km^2 of the total catchment area (285 km^2), mainly consisting of mica-schist and paragneiss. The discharge of Riegerbach is generally highest in spring and early summer due to snowmelt (Schulz, 1971). All other relevant inflows enter the lake along its north-eastern shoreline, where they led to the formation of several fan systems, e.g. at Millstatt and Pesenthein. These fans protrude far into the lake and separate it into three main basins: the north-western basin (up to 106 m deep), the middle basin (122 m) and the south-eastern basin (137 m). The northwest-southeast elongated lake is bordered by steep (25–30°) lateral slopes. The outflow of the lake in the northwest drains the lake into the Drau valley. Due to its depth and wind-protected position in between mountain ridges, the water body of Millstätter See only mixes to depths of about 50 m during spring and autumn (Findenegg, 1933), leading to oxygen depletion throughout the basin deep. Similar to Wörthersee, eutrophication led to increased calcite precipitation and oxygen depletion in the deep basins during the 1960s and 1970s (Sampl, 1976). In summertime, the summits northeast of Millstätter See are often subject to storms and intense rainfall, occasionally causing the usually calm creeks to swell rapidly. In 1958 CE such an event led to severe debris flows and floods in Millstatt and Pesenthein, which destroyed 83 houses and 13 cars and caused seven casualties. Moreover, an estimated 3×10^5 m^3 of debris flushed into the lake and parts of the shoreline collapsed (Schwarzl, 1971).

3. Methodology

3.1. Macroseismic intensity of past earthquakes

To calibrate the lacustrine sediment archives with historically and instrumentally recorded earthquakes, we gathered information on macroseismic intensities at our lake sites from different sources. The majority of the data results from entries in the SHARE European Earthquake Catalogue (SHEEC; Stucchi et al., 2013). This community-driven archive supplies information about individual historical earthquakes by integration of different national databases. For most earthquakes considered in this study, the catalogue of strong earthquakes in Italy and in the Mediterranean (CFTI5med; Guidoboni et al., 2019) comprises the most comprehensive data. The different data sources provide macroseismic intensities either in the MCS, the MSK or the European Macroseismic Scale (EMS-98; Grünthal et al., 1998). Given that the scales are roughly equivalent to one another (Musson et al., 2010), no conversion is required for

epicentres given in literature are plotted: close to the Katschberg fault (1201 CE a; Hammerl, 1995) and near Murau (1201 CE b; Alexandre, 1990). **(b)**–**(f)** Historically reported macroseismic intensity data points (IDPs; EMS-98 scale) of large earthquakes that affected the study area. IDPs for the 1348 CE and the 1690 CE earthquake are provided by the SHEEC 1000–1899 (Stucchi et al., 2013). To calculate possible macroseismic intensities at our lake sites for the 1511 CE event, the IDPs given by Camassi et al., (2011) were interpolated (Section 3.1, supplementary data 1). The intensities of the 1857 CE earthquake at the lake sites result from interpolation of IDPs derived from historical reports (supplementary data 2). The vast amount of IDPs for the 1976 CE earthquake is provided by Tertulliani et al. (2018).

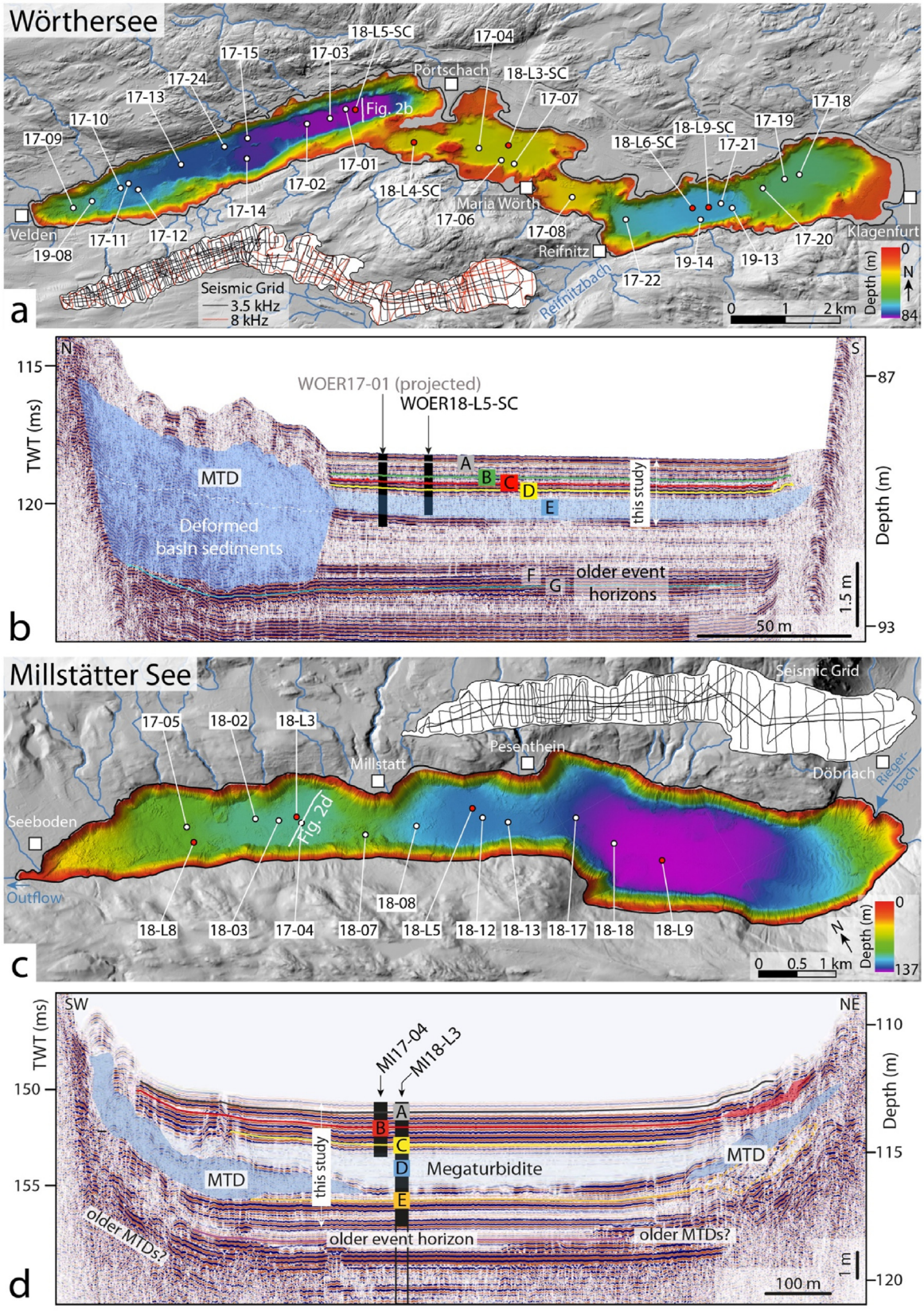

Fig. 2. Bathymetric maps and representative seismic profiles of Wörthersee (a, b) and Millstätter See (c, d). Core locations are indicated as white (short hammer cores) and red (long Kullenberg cores) dots. The core labels (e.g. "17−04") were abbreviated and do not include the lake-specific prefix ("WOER" for Wörthersee and "MI" for Millstätter See). Traces of all acquired acoustic seismic profiles are shown on the insets of Fig. 2a and c. A detailed description of the seismic stratigraphy of both lakes is given in supplementary data 3 & 4. **(a)** Bathymetric map of Wörthersee. **(b)** Seismic profile (8 kHz) from the deepest part of Wörthersee, perpendicular to the lake axis (see Fig. 2a for location). Five seismostratigraphic horizons of MTDs (event horizons, EH; labelled A-E) are present in the uppermost ~1.5 m. **(c)** Bathymetric map of Millstätter See. **(d)** Seismic profile (3.5 kHz) across the north-

the purpose of this study. Similar to previous studies concerning the calibration of lacustrine paleoseismic archives (e.g. Moernaut et al., 2014; Van Daele et al., 2015), we use the term "seismic intensity" as a measure of seismic shaking strength. To calibrate the sedimentary imprint accurately for different lake basins and to account for spatial variability of shaking strength, we used one-fourth fractions of an intensity degree.

For the 1348 CE earthquake, Guidoboni and Comastri (2005b) and Guidoboni et al. (2019) report an I_L of VIII – IX at Reifnitz, located directly at the shore of Wörthersee. Given the broad distribution of IDPs around Wörthersee with I_L > VIII, we decided to attribute the intensity range of VIII – IX to all lake basins (Table 1). For Millstätter See, we use the value of an IDP (VIII – IX) obtained less than 3 km southwest of the lake. For the 1511 CE event, the intensities in Carinthia are poorly constrained. A datapoint from Villach (VII–VIII) as well as several datapoints north of the study area (e.g. V–VI in Vienna) are available in literature (Camassi et al., 2011). We calculated possible intensities at our lake sites by interpolating the existing IDPs (Kriging interpolation). For locations in Germany, where the earthquake was felt, an I_L of II½ was assumed. The resulting intensities are ~ VII¼ to VII½ at both lake sites. We also calculated intensities based on a local (Austrian) intensity prediction equation (IPE; Papí Isaba et al., 2020) and a Swiss IPE (Fäh et al., 2011), applied to the estimated epicentre location and magnitude of these events given by Stucchi et al. (2013) (see supplementary data 1). To account for epistemic uncertainties, we used a combination of both IPEs with equal weighting. Italian IPEs were not considered, because they are based on heterogeneous datasets from the Apennine and the Alps combined (e.g. Peruzza, 1996; Albarello & D'Amico, 2004; Pasolini et al., 2008). As the distance from the estimated epicentre to both lakes is similar (~73 km to Wörthersee, 67 km to Millstätter See) this provides intensity ranges from VI¾ to VII¾ for both lakes, thus encompassing the intensities provided by IDP-interpolation. To account for uncertainties caused by the scarcity of IDPs inside and north of the study area, we hereafter use the wider range of I_L provided by the IPEs. The seismic intensities of the 1690 CE earthquake are well constrained in the study area: IDPs are available from Millstatt and Klagenfurt (VII-VIII; Stucchi et al., 2013). By interpolating linearly between an IDP close to Villach (VIII-IX) and the one in Klagenfurt, we derive slightly varying intensity ranges at the Wörthersee subbasins. For the 1857 CE event, a set of new IDPs was established by comprehensive investigation of historical reports (see supplementary data 2). For the recent 1976 CE earthquake, a vast amount of IDPs is available (Tertulliani et al., 2018).

3.2. Bathymetry and reflection-seismic data

On Wörthersee, a SeaBat T50-P multibeam echosounder in combination with an AsteRx-U MARINE GNSS Heading System was used to acquire bathymetric data in 2017. On Millstätter See, bathymetric data were acquired in 2019 using a Kongsberg EM2040 multibeam echosounder (300 kHz, 1° beam width). Positioning was carried out with a Leica GX 1230+ GNSS receiver combined with real-time kinematic positioning service EPOSA (RTK, VRS). Bathymetric maps of 2 m (Wörthersee) or 1 m (Millstätter See) grid cell size were generated using QGIS software v. 3.4.15 (QGIS Development Team, 2018). To enhance visibility of morphological features, topographic openness (Yokoyama et al., 2002) was calculated in SAGA GIS (Conrad et al., 2015).

High-resolution reflection seismic data were acquired during several surveys between 2017 and 2019, using a 3.5 kHz Kongsberg Geopulse pinger source with a theoretical vertical resolution of ~10 cm. On Wörthersee, an Innomar SES-2000 light subbottom profiler (100 kHz primary frequency, 8 kHz secondary frequency) with a theoretical vertical resolution of ~5 cm was used as well. Positioning during seismic surveys was carried out with standalone GPS. The data were processed in the IHS Markit Kingdom (v. 2020) software. For the 3.5 kHz data, a bandpass filter with a lower cut of 2 kHz and an upper cut of 6 kHz was applied.

Bodies with basinward-thinning geometries and chaotic or irregular seismic facies were identified as MTDs following Sammartini et al. (2019). They are often overlain by homogenous, semi-transparent units with a ponding geometry. This seismic facies is attributed to megaturbidites sensu Schnellmann et al. (2006). Both landslide-related deposits (MTDs and megaturbidites) differ strongly from regular background sedimentation, which is characterized by continuous reflections. To recognise synchronous deposition of MTDs (within the limits of seismic resolution), their equivalent seismic-stratigraphic horizons were mapped over the lake basins. For inter-basin-correlation of seismic-stratigraphic horizons, correlation polygons were used and visually matched with the seismic-stratigraphic sequence. Time-to-depth conversion was carried out assuming a constant acoustic velocity of 1500 m/s for both water and sediment. In figures showing seismic profiles, two-way travel time (TWT) of the seismic wave in milliseconds (ms) is given as well.

3.3. Sediment core analysis

Short (~1.5 m) sediment cores were taken during several surveys between 2017 and 2019 using a gravity corer with a manual percussion system. Long sediment cores (~11 m) in Millstätter See were retrieved in 2018 with a modified Kullenberg gravity piston coring system (Kelts et al., 1986) and cut into 1.5 m sections. On selected cores, X-ray computed tomography (CT) scans were carried out either on whole round (Wörthersee) or split sediment cores (Millstätter See) at the Medical University of Innsbruck, using a Siemens SOMATOM Definition AS (voxel size 0.2 × 0.2 × 0.3 mm). Sediment physical property data was acquired at the Austrian Core Facility (Institute of Geology, University of Innsbruck): γ-Density (5 mm resolution) and magnetic susceptibility (2–3 mm resolution) were measured with a GEOTEK Multi-Sensor Core Logger (MSCL) and a Bartington MS2E point sensor.

Grain size analysis was carried out using laser diffractometry (Malvern Mastersizer 3000) on bulk samples at varying sampling intervals. At the base of event deposits, sampling intervals down to 2 mm were chosen. For the intervals of thick event deposits (megaturbidites) considered ± homogeneous, samples were taken in intervals of 5–10 cm, depending on the overall thickness of the deposit. To aid sample disaggregation, ultrasonication of 40% was applied for 40 s.

For microfacies analyses and establishing high-resolution age models based on varve counting, sediment thin sections were prepared following the procedure described in e.g. Lamoureux (1994). Turbidite deposits were identified in the sediment cores and on thin sections based on their texture and composition (e.g. grading and/or generally homogeneous appearance, increased amount of detrital grains, large organic macro-remains) that contrast with the finely laminated background sediments (Sections

western basin of Millstättersee (see Fig. 2c for location). Five EHs (A–E) can be distinguished in the uppermost 5 m. The short sediment cores (e.g. MI17-04) barely reach down to EH-D, while the long cores (e.g. MI18-L3) cover all EHs discussed in this paper. (For interpretation of the references to colour in this figure legend, the reader is referred to the Web version of this article.)

Table 1
Seismic intensities of large earthquakes at the lake (sub)basins. M_w is given according to the SHEEC 1000–1899 (Stucchi et al., 2013) and Tertulliani et al. (2018) (for 1976 CE).

		Intensity (EMS-98) at lake site				
Earthquake (CE)	M_w	Wörthersee W	Wörthersee Mid	Wörthersee E	Millstätter See	Sources
1348	6.99 ± 0.3	VIII-IX	VIII-IX	VIII-IX	VIII-IX	Guidoboni et al. (2019); Stucchi et al. (2013)
1511	6.89 ± 0.3	VI¾-VII¾	VI¾-VII¾	VI¾-VII¾	VI¾-VII¾	Camassi et al. (2011); Supplementary data 1
1690	6.56 ± 0.3	VII½-VIII½	VII½-VIII½	VII¼-VIII¼	VII-VIII	Guidoboni et al. (2019); Stucchi et al. (2013)
1857	5.14 ± 0.5	V½-VI	V¼-V¾	IV¾-V¼	< V	Supplementary data 2
1976	6.4	V½	V	V	V½	Tertulliani et al., (2018)

4.1.3 and 4.2.3). For thick (~30 cm or more) turbidites that are also mappable on seismic profiles, we use the term "megaturbidite" (cf. Bouma, 1987; Schnellmann et al., 2006).

3.4. Chronology

AMS radiocarbon measurements were performed on terrestrial organic macro-remains at the Ion beam Physics Laboratory of ETH Zürich and calibrated using the IntCal20 calibration curve (Reimer et al., 2020).

Short-lived radionuclide activity (^{210}Pb and ^{137}Cs) was measured at Eawag Dübendorf, Switzerland, using *CANBERRA* and *Princeton Gamma-Tech* germanium well detectors. To assess recent sedimentation rates and date the uppermost sediments, a constant flux/constant sedimentation (CFCS) model was used in the R package *serac* (Bruel and Sabatier, 2020). All samples were collected from background sediment (i.e. finely laminated sediment) and intervals of remobilized sediment (turbidite deposits >1 mm) were omitted.

After testing the finely laminated sediment sections for being seasonal (see Sections 4.1.2 and 4.2.2), varve counting (e.g. Zolitschka et al., 2015) was carried out on thin sections using both plane- and cross-polarized light. Introducing colour contrast to polarized images with a red tint plate (gypsum) generally proved to be useful for varve recognition. Each thin section was subdivided into subsections of typically 2–5 cm length, bordered by easily recognizable markers (e.g. detrital layers). These subsections were then counted at least 3 times, visually integrating over the whole width of the thin section to circumvent potential varve disturbances. For the final age-depth-model, the average of the counts was retained. The relative counting errors are given as the standard deviation (1σ if not stated otherwise) of the multiple counts, giving a measure for the precision of the varve chronology. To detect chronological errors due to internal disturbances (e.g. possible hiatuses in case of erosion at the base of turbidites), varve counts were performed on several cores from the same basin (Wörthersee) and/or verified by radionuclide (^{14}C, ^{210}Pb and ^{137}Cs) dating.

In intervals with insufficient varve preservation (mainly due to lower sedimentation rates), the varve age model was extended by interpolation between the lowermost counted varve and the following absolute age to cover the time interval presented in this study. Where ^{14}C-ages were available, the varve counting uncertainty was interpolated between the uncertainty of the lowermost counted varve to the 95% range of the following calibrated ^{14}C date.

4. Results

4.1. Wörthersee

4.1.1. Seismic-stratigraphic event horizons

The general seismic stratigraphy of Wörthersee consists of two main seismic units (SUs; Daxer et al., 2020). In both SUs, the regular sedimentation, indicated by continuous parallel reflections, is interrupted by MTDs. These MTDs are assigned to distinct event-stratigraphic horizons (EH). The three most prominent EHs, the two younger of which (EH-A and EH-E in Fig. 2b) are within in the scope of this study, were already described and dated by Daxer et al. (2020). Based on the high vertical resolution (~5 cm) of the 8 kHz data, we were able to map three additional EHs that comprise either multiple (EH-B & EH-C) or single (EH-D) MTDs. A ~50 cm thick megaturbidite that covers most of the western basin is associated with the MTDs of EH-E (Fig. 2b). A detailed description of the seismic stratigraphy is provided in supplementary data 3.

4.1.2. General lithology and chronology

In the western and the eastern basin, the uppermost 2 m of the sedimentary succession (corresponding to the scope of this study) consist of annually laminated sediments (varves), as confirmed by independent short-lived radionuclide (^{210}Pb, ^{137}Cs) and radiocarbon dating (Fig. 3a, b, c). In the middle basin, laminated sediments are restricted to the uppermost ~10 cm of the succession. Based on presence/absence of laminations and varve composition/preservation, the sediments can be divided into five different lithotypes (LTs). LTs Ia, Ib and Ic are well to faintly laminated (at least on a microscopical level), whereas LTs IIa and IIb lack laminae.

The annual sediment couplets of LT Ia are 0.5–1 mm thick (Fig. 3b). They consist of a bright lamina of abundant authigenic calcite deposited in early summer, and a darker lamina of diatoms and amorphous organic matter deposited in fall (Fig. 3d). In LT Ib, varve thicknesses are in the range of 0.3–1 mm. The main components of the summer/fall layers of LT Ib are amorphous organic matter, diatoms, and interspersed clastic material, while authigenic calcite is relatively sparse (Fig. 3d). The winter layers of LT Ib are characterized by bright lamina of fine silt – to clay-sized minerals. Organic-rich varves are also present in LT Ic, but the laminae are often distorted and thinner (0.1–0.4 mm) than in LT Ib.

LT IIa and LT IIb are non-laminated sediments only present in cores from the middle basin and the shallower parts of the eastern basin. LT IIa is homogeneously dark in appearance and mainly consisting of fine-grained mud with abundant organic macro-remains and amorphous organic matter (Fig. 3c). The bright macroscopic appearance of LT IIb is caused by high amounts of authigenic calcite, similar to LT Ia, but lacking distinct laminations.

The well-preserved varves of LT Ia and Ib allowed the construction of independent age-depth models for the uppermost ~50 cm in several cores from the western and eastern basin (Fig. 3a, b, c). Relative counting errors are in the range of 3–5% (1σ). In LT Ia, counting could also be performed by the unaided eye on high-resolution core images (Fig. 3b). In LT Ic, counting on sediment thin sections was partly possible, but errors are generally higher (~10%) due to poor varve preservation. The average background sedimentation rates are 1.35 mm/yr in LT Ia, 0.65 mm/yr in LT Ib and 0.4–0.5 mm/yr in LT Ic. The low sedimentation rate of the non-laminated LT IIa could be constrained to <0.25 mm/yr by core-to-core correlation (Fig. 3c and supplementary data 5 & 6).

The regular background sedimentation is frequently interrupted

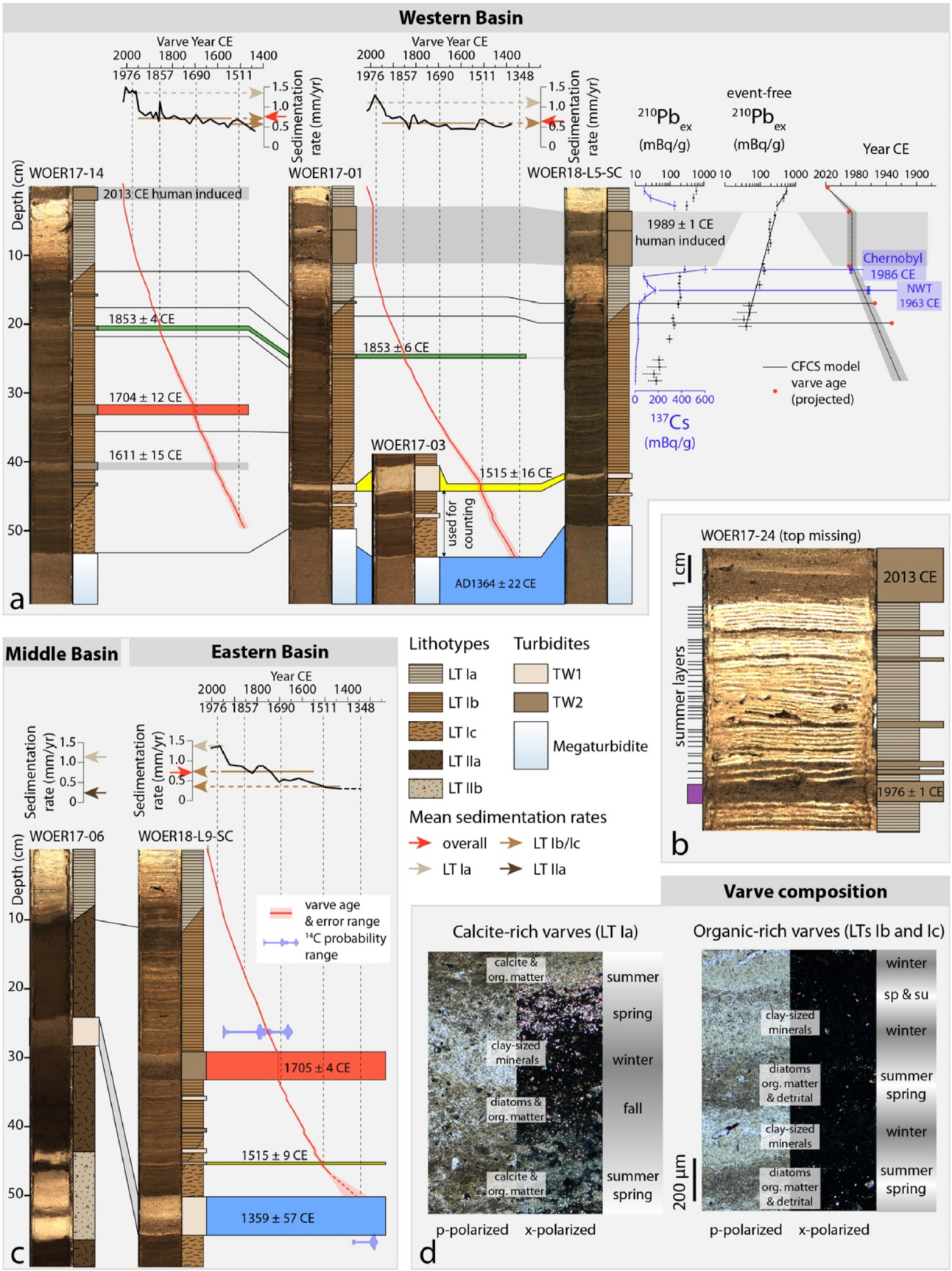

Fig. 3. Lithology and age-depth models of Wörthersee sediment cores. **(a)** The age-depth models from the western basin suggest that the major earthquakes are archived in the sedimentary record as cm-to dm-scale turbidites. **(b)** The well-laminated sediments of lithotype (LT) Ia in core WOER17-24 allow varve counting by the unaided eye. The turbidite at

by mm-to dm-scaled turbidites. In the western basin, the thickest turbidites date to 2013 ± 0, 1989 ± 1, 1976 ± 1, 1853 ± 6, 1704 ± 12, 1611 ± 15, 1515 ± 16, and 1364 ± 22 CE. In the eastern basin (core WOER18-L9-SC), two outstanding turbidites date to 1705 ± 4 and 1359 ± 57 CE, while a thin (0.6 cm) turbidite has a varve age of 1515 ± 9 CE. In the middle basin (core WOER17-06), only one cm-scale turbidite is present in the uppermost 50 cm of the sedimentary succession. Correlation to core WOER18-L9-SC suggests that this turbidite is time-equivalent to the turbidite dated to 1359 ± 57 CE (Fig. 3c; see also Section 4.1.4 and supplementary data 6). The two most recent turbidites (2013 and 1989 ± 1 CE correspond to seismostratigraphic EH-A and originated from human-induced landslides; Daxer et al., 2020).

4.1.3. Types of turbidites

Based on colour, magnetic susceptibility, grain-size characteristics and microfacies, we discriminate three types of lacustrine turbidites in Wörthersee: calcite-rich turbidites (turbidite Wörthersee 1, TW1), clastic-organic-rich turbidites (TW2), and megaturbidites. Thickness, grain size distribution and macroscopic appearance of single turbidites are dependent on the coring site in relation to the sediment source. We therefore distinguish proximal and distal deposits for TW1 and TW2 (see section 4.1.4 for details on source and transport direction of deposits). Proximal TWs are deposited close to their causative landslide/MTD and therefore relatively thick (>3 cm). The deposition of distal TWs occurs at a comparatively long distance from the associated mass movement, leading to rather thin (<~1 cm) turbidites.

Calcite-rich TW1s are characterized by high reflectivity and lower magnetic susceptibility than the background sedimentation. The base of proximal TW1s consists of fine sand and gradually fines into a homogeneous silty top. Distal TW1s are homogeneous throughout the whole turbidite and consist of very coarse silt (Fig. 4). Large organic macro-remains (leaves and needles) and fragments of gastropod shells are common in the basal part of proximal TW1s. The bright colour and low magnetic susceptibility are due to abundant authigenic calcite.

Clastic-organic-rich TW2s show magnetic susceptibilities higher or similar to the background sediment due to varying amounts of siliciclastic mineral grains (quartz, mica, feldspar). In proximal TW2s, sand-sized particles and considerable amounts of organic remains are visible macroscopically. The microfacies of distal TW2s is either dominated by clastic, silt-sized grains with a slight upward-fining trend or a mixture of amorphous organic matter and calcite-rich background sediment. Other than in TW1s, however, calcite is not the major constituent, resulting in dark-coloured turbidites.

The only megaturbidite present in the studied interval of Wörthersee is attributed to the 1348 CE earthquake (Daxer et al., 2020, Figs. 3 and 4). It is considerably thicker (up to ~30 cm) than TW1s and TW2s and consists of a coarse-grained (silt to sand) base and a thick, homogeneous interval of silt on top. The composition of the megaturbidite base resembles that of TW1s and often shows macroscopically visible fluctuations in colour and grain-size, indicating amalgamation of several individually triggered turbidites. Amalgamation of turbidity currents also occurred during the deposition of the TW2s dated to 1853 ± 6 and 1704 ± 12 CE (Fig. 4). These TW2s are composed of a succession of individual turbidites that differ in the amount of detrital grains, organic matter and/or authigenic calcite.

4.1.4. Core-to-core and core-to-seismic correlation

The distinct changes of lithotypes, variations in magnetic susceptibility and turbidites as marker layers allow accurate core-to-core correlations (Fig. 5, supplementary data 5 & 6). The inter-basin correlations are further corroborated by the age-depth models and radiocarbon ages (Figs. 3 and 5). For the events of 1364 ± 22, 1515 ± 16 and 1704 ± 12, turbidites are present in both the western and the eastern basin, while the events of 1853 ± 6 and 1976 ± 1 only left their traces in the western basin.

The core-to-seismic correlation in Wörthersee is mainly based on the megaturbidites of EH-E, which correspond to the ~30 cm thick turbidite of the event dated to 1364 ± 22 CE as well as spatial considerations of smaller-scale turbidites. Proximal turbidites are relatively thick and coarse-grained, thus differing strongly in density from the surrounding background sediment. Distal turbidites, however, are thin and fine-grained, and density contrasts therefore are small. In the seismic data, the seismostratigraphic horizons show high-amplitude reflections close to the respective MTDs that fade out distally. This allows for a reliable attribution of mapped MTDs to the well-dated turbidites in the sediment cores. The resulting correlation indicates that (i) EH-A corresponds to the event deposits dated to 2013 and 1989 ± 1 CE, respectively, (ii) EH-B corresponds to the turbidite of 1853 ± 6 CE, (iii) EH-C corresponds to the turbidites dated to 1704 ± 12 (western basin) and 1705 ± 4 (eastern basin) and (iv) EH-D corresponds to the turbidites dated to 1515 ± 16 (western basin) and 1515 ± 9 (eastern basin), respectively. A detailed seismic-to-core correlation is provided in supplementary data 7.

4.2. Millstätter See

4.2.1. Seismic-stratigraphic event horizons

In the uppermost 5 m of the seismostratigraphic succession of Millstätter See, five horizons (labelled A-E) of mass-transport deposits are present (Fig. 2d). All these event horizons comprise at least two MTDs. The MTDs of EH-D reach maximum thicknesses of 11 m and are overlain by an up to ~140 cm (1.8 ms) thick megaturbidite that covers all basin depocenters (Fig. 2d). A detailed description of the seismic stratigraphy is provided in supplementary data 4.

4.2.2. General lithology and chronology

Throughout the whole cored interval, the background sediments of Millstätter See are laminated on a mm to sub-mm scale. The annual character of the laminations is confirmed by short-lived radionuclide and radiocarbon dating (Fig. 6). The period of eutrophication in the ~1960s is reflected in increased calcite contents, leading to brighter colours at ~10 cm core depth. A typical varve consists of a brown, organic rich summer layer and a bright winter layer of fine silt-to clay-sized particles (Fig. 6b). The summer layers often show an enhanced amount of detrital minerogenic content, which is attributed to high runoff events during spring snowmelt and local summer storms. Depending on the amount and thickness of these detrital intervals, varve thickness varies strongly. At the transition from summer to winter layers, a high number of centric diatoms is often present.

The continuously varved record of Millstätter See allows the

the core top was caused by onshore building action in December 2013 (Daxer et al., 2020). **(c)** The thickest turbidites in the eastern basin date to 1705 ± 4 CE and 1359 ± 57 CE. In the middle basin, only one prominent turbidite is present. Core correlation (Section 4.1.4) suggests that this turbidite corresponds to the turbidite of 1359 ± 57 CE in the eastern basin. **(d)** Varve composition of lithotypes Ia and Ib. Summer layers of LT Ia are rich in calcite (bright colours under cross-polarized light) and organic matter. In LT Ib, calcite is mostly absent. Winter layers of both lithotypes are composed of clay-to silt-sized minerogenic particles. (For interpretation of the references to colour in this figure legend, the reader is referred to the Web version of this article.)

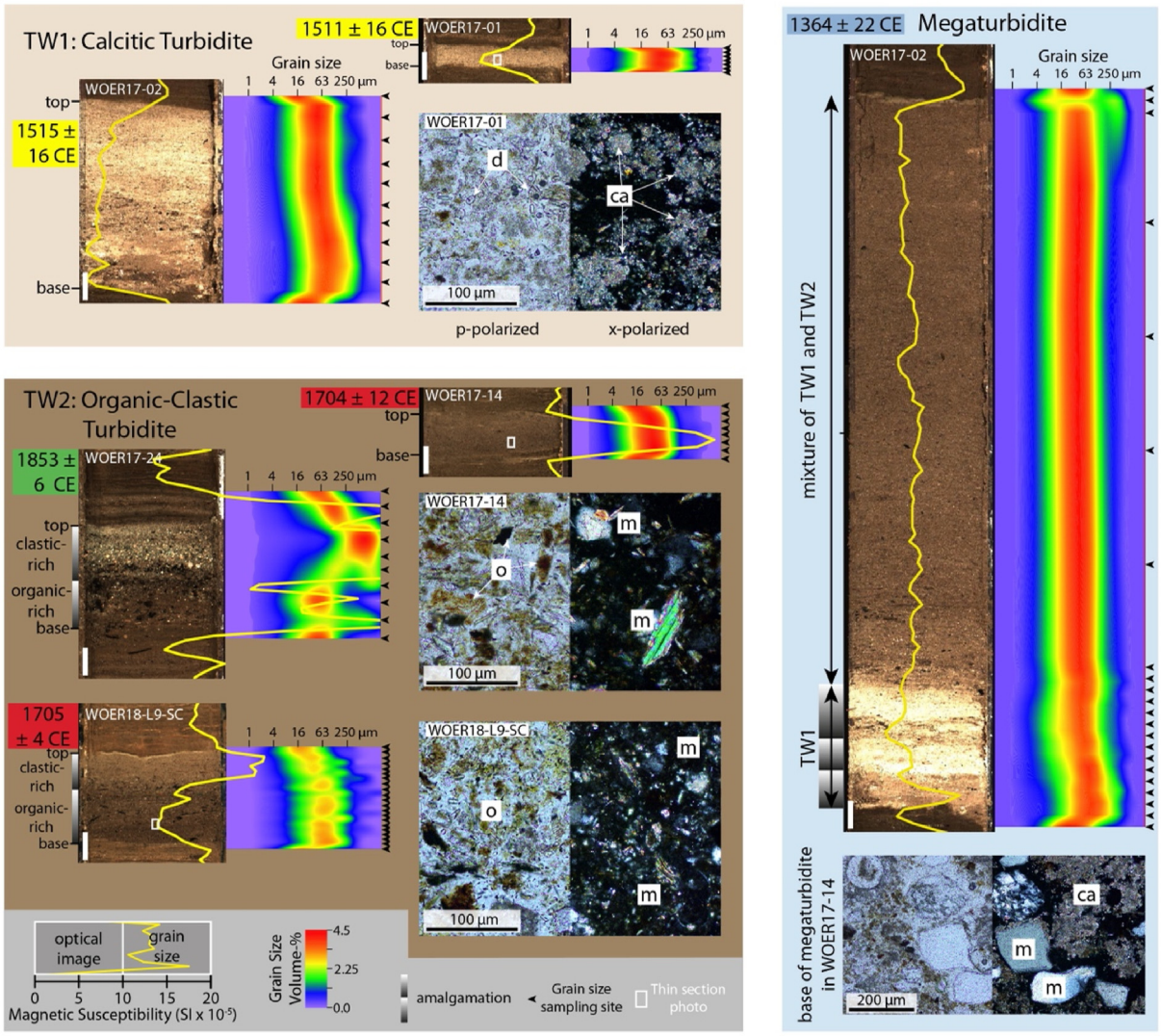

Fig. 4. Types of turbidites in Wörthersee. Based on their composition and thickness, we discriminate three types of turbidites: calcitic turbidites (TW1), organic-clastic turbidites (TW2) and megaturbidites. TW1s are characterized by macroscopically bright colours and low magnetic susceptibility due to high authigenic calcite content (ca in microscopical image) and diatoms (d). TW2s are rich in organic matter (o) and minerogenic grains (m) and therefore show large fluctuations in magnetic susceptibility and grain size. Megaturbidites are characterized by a coarse-grained base and a mixture of minerogenic grains, authigenic calcite and organic matter. The white vertical bars correspond to 1 cm. (For interpretation of the references to colour in this figure legend, the reader is referred to the Web version of this article.)

construction of a highly precise age-depth model (Fig. 6a). Because core handling disturbances due to high amounts of pore-water prohibited varve counting on thin sections in the uppermost ~10 cm, the varve-based age-depth model was tied to the nuclear weapon test peak in the ^{137}Cs profile. This introduces some additional uncertainty (±3 years) in the otherwise very precise age-depth model (<2% relative counting error). The age depth model confirms very stable background sedimentation rates of 1.5 mm/yr throughout the cored interval. The overall sedimentation rates in the last ~600 years are almost twice as high as in Wörthersee due to numerous (sub)mm-scale detrital layers. The two most prominent turbidites in core MI17-04 date to 1686 ± 8 and 1350 ± 10 CE.

4.2.3. Types of turbidites

The turbidites of Millstätter See can be separated into four main types: lacustrine turbidites with a composition equal to background sediments (TM1), lacustrine turbidites with a clastic-organic composition (TM2), mixtures thereof (TM1/2) and megaturbidites.

The only TM1 in core MI17-04 dates to 1686 ± 8. It is 6 cm thick and shows magnetic susceptibility values comparable to background sediment (Fig. 7). It is composed of three units: a fine-grained basal unit (~1 cm thick), a slightly coarser middle unit (~4 cm thick) and a small, very bright top unit consisting of fine silt. The basal unit and the middle unit can also be distinguished in the microfacies: the basal unit consists of background sediments (diatoms, fine-grained detrital clastics) and interspersed organic matter. In the middle unit, distinct yellow sediment aggregates consisting of diatoms and silt-sized particles (typical of winter laminae) are dominant, while organic matter is scarce. This separation of units and the overall turbidite composition suggest amalgamation of turbidity currents with different hemipelagic sources.

Clastic-organic turbidites (TM2; Fig. 7) show a coarse sandy base overlain by a finer, homogeneous, or fining upward interval. Especially in areas close to the alluvial fans, TM2s are very coarse grained. Compared to TM1s, the amount of organic matter and minerogenic particles (especially mica) is higher, whereas

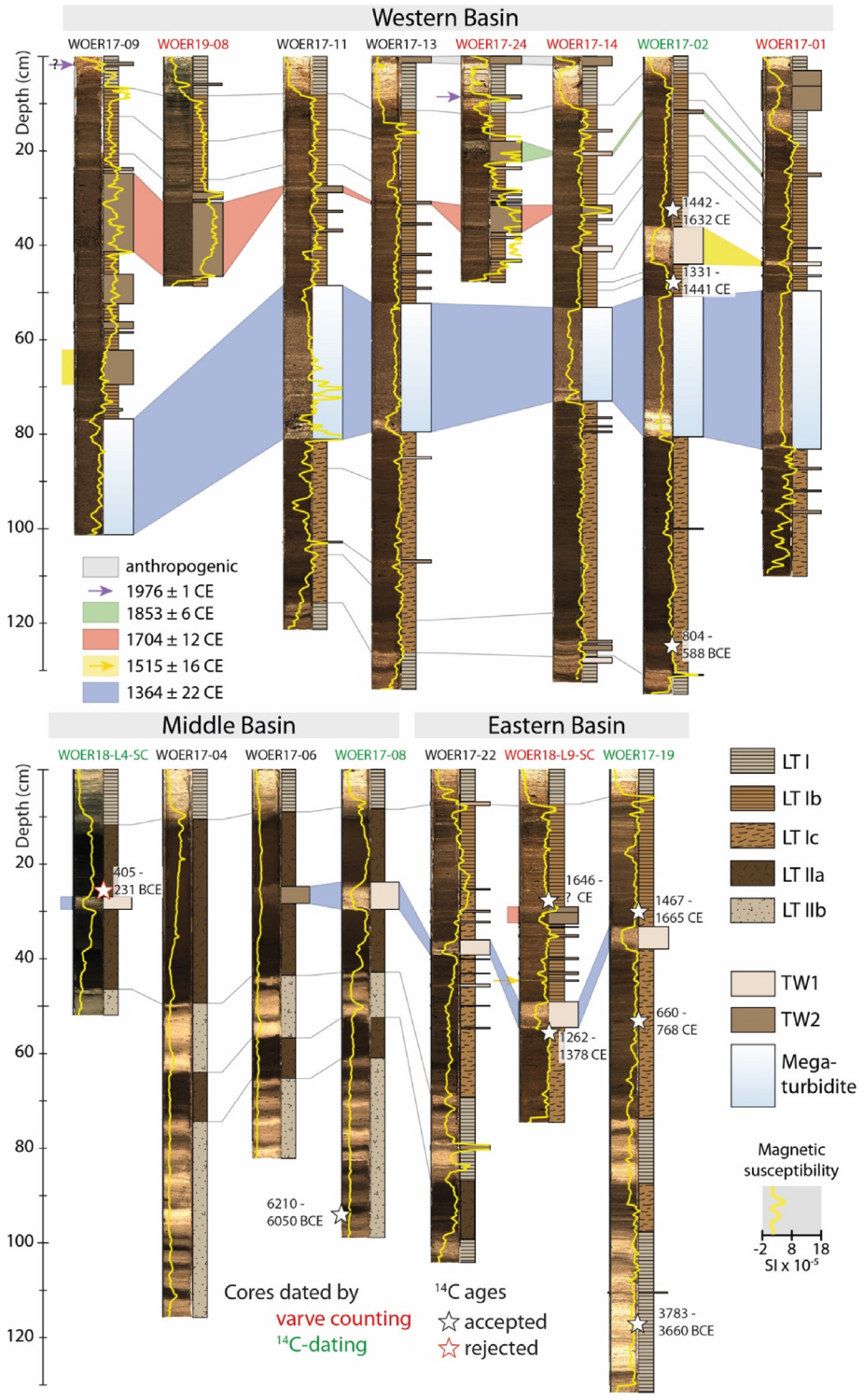

Fig. 5. Correlation of sediment cores from Wörthersee. A correlation of all short sediment cores is provided in supplementary data 5 & 6.

background sediment patches are absent or subordinate. This is also reflected in higher and/or strongly fluctuating magnetic susceptibility values. TM2s with a coarse-grained base and a gradual fining upward trend are often stacked on top of each other.

While most turbidites correspond to type TM2, some turbidites show a mixed composition consisting of mineral grains, organic matter, and background sediment patches (TM1/2). Depending on the relative amounts of these constituents, magnetic susceptibility is highly variable. One of these "mixed" turbidites in core MI17-04 dates to 1517 ± 9 CE and sticks out from all other small-scale (<5 cm) turbidites, because it shows amalgamation of two individual turbidites (Fig. 7). The lower turbidite mainly consists of yellowish background-sediment patches and minerogenic particles. The base of the upper turbidite is characterized by an almost

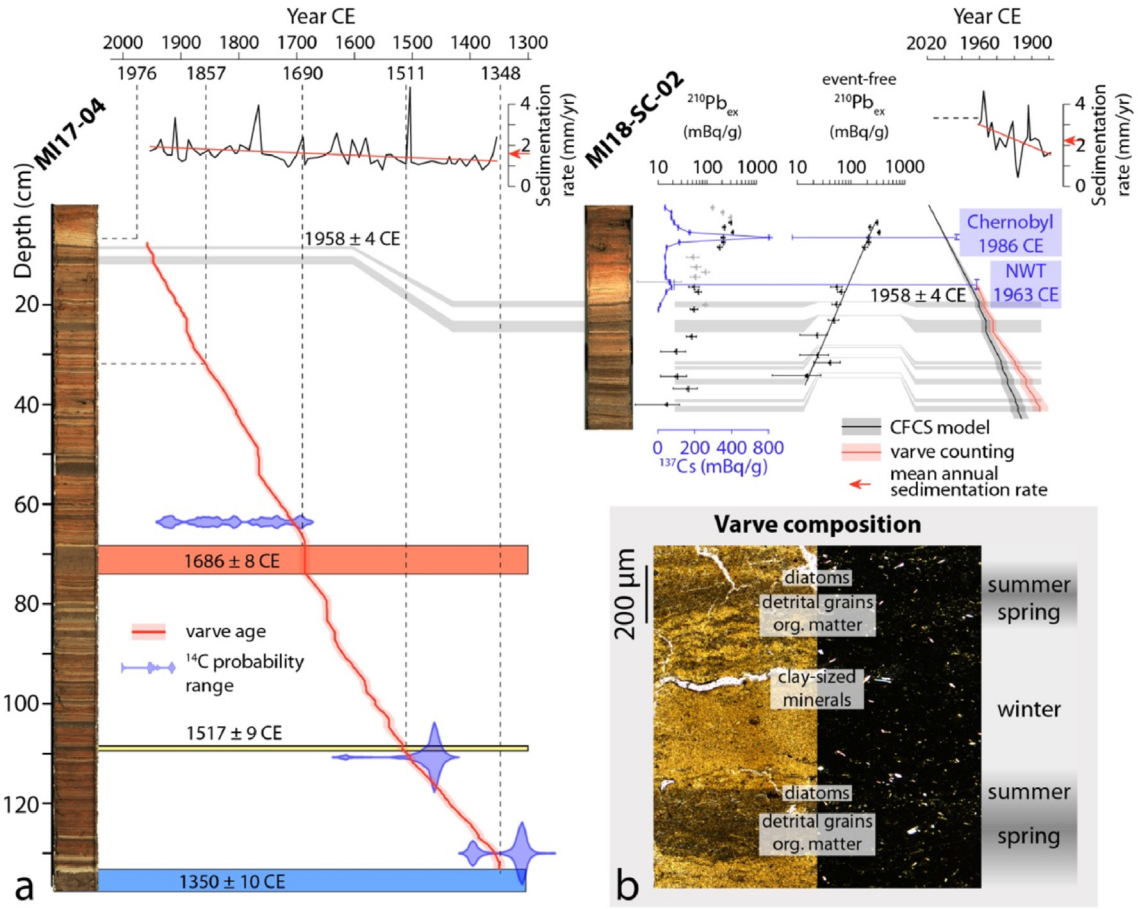

Fig. 6. Age-depth model and background sediment characterization of Millstätter See. **(a)** A highly accurate age-depth model was constructed by varve counting and independently confirmed by short-lived radionuclide (^{210}Pb and ^{137}Cs) and radiocarbon dating. Because of core disturbances at the top of cores MI17-04 and MI18-SC90-02, the varve count was tied to the ^{137}Cs peak of 1963, caused by nuclear weapon tests (NWT). The image of core MI17-04 was stretched horizontally to aid visibility. **(b)** The background sediments of Millstätter See are characterized by organic-clastic varves. The spring and summer layers show enhanced amounts of detrital grains, diatoms, and organic matter (leading to a characteristic brown colour). In winter, mainly clay-sized minerals are deposited. (For interpretation of the references to colour in this figure legend, the reader is referred to the Web version of this article.)

purely minerogenic composition, leading to higher CT-densities (red arrow in Fig. 7).

Similar to Wörthersee, the fourth type of turbidites differs strongly from TM1s and TM2s in terms of thickness. The only megaturbidite in the sediment cores of Millstätter See is up to ~2 m thick and dates to 1350 ± 10 (Fig. 8). It consists of a multi-pulsed (amalgamated) coarse-grained base, a homogeneous middle part resembling TM1s in composition and comprising most of the turbidite, and a white clay-cap (Fig. 7).

4.2.4. Core-to-core and core-to-seismic correlation

The major turbidites in Millstätter See can be traced over the lake basins by accurate core-to-core correlation (Fig. 8; supplementary data 8). The megaturbidite of 1350 ± 10, which corresponds to EH-D, is the main link between seismic and sediment core data. The resulting correlation (supplementary data 9 & 10), which is also based on the relative stratigraphic position and the spatial distribution of turbidites (see chapter 5.1.2), shows that (i) the turbidite dated to 1958 ± 4 CE can be reliably linked to at least two MTDs of EH-A, (ii) EH-B corresponds to the turbidites of 1686 ± 8 CE, (iii) EH-C corresponds to the turbidites dated to 1517 ± 9 CE and (iv) EH-E corresponds to turbidites dated to ~1350–1100 CE by radiocarbon dating (Fig. 8).

5. Discussion

5.1. Assessing the lacustrine imprint of earthquakes

5.1.1. Turbidite composition and potential triggering mechanisms

In Wörthersee and Millstätter See, turbidites with a dominant (TW1s, TM1s and megaturbidites) or partly (TM1/2s) lake-internal composition can be distinguished from turbidites with a high amount of terrestrial components (TW2 and TM2). TW1s mainly consist of gastropod shells and authigenic calcite, indicating that the source area of these turbidites are low energy littoral environments with minor alluvial influence (cf. Valero-Garcés et al., 2014). The composition of TM1s (diatoms and fine-grained clastic components) corresponds to background sediments in Millstätter See that are deposited far from alluvial fans, e.g. on hemipelagic slopes and in the basin flats. We therefore interpret TW1s, TM1s, TM1/2s and megaturbidites to be related to landslides originating from non-deltaic sublacustrine slopes. Failure of these lateral slopes is usually caused by an external triggering mechanism, such as an earthquake or human-induced loading along the shoreline (cf. Sammartini et al., 2019). TW2s and TM2s, on the other hand, are rich in macro-organic matter and coarse-grained minerogenic components that reflect catchment lithology, indicating that the source of these turbidites is close to river inflows. Possible

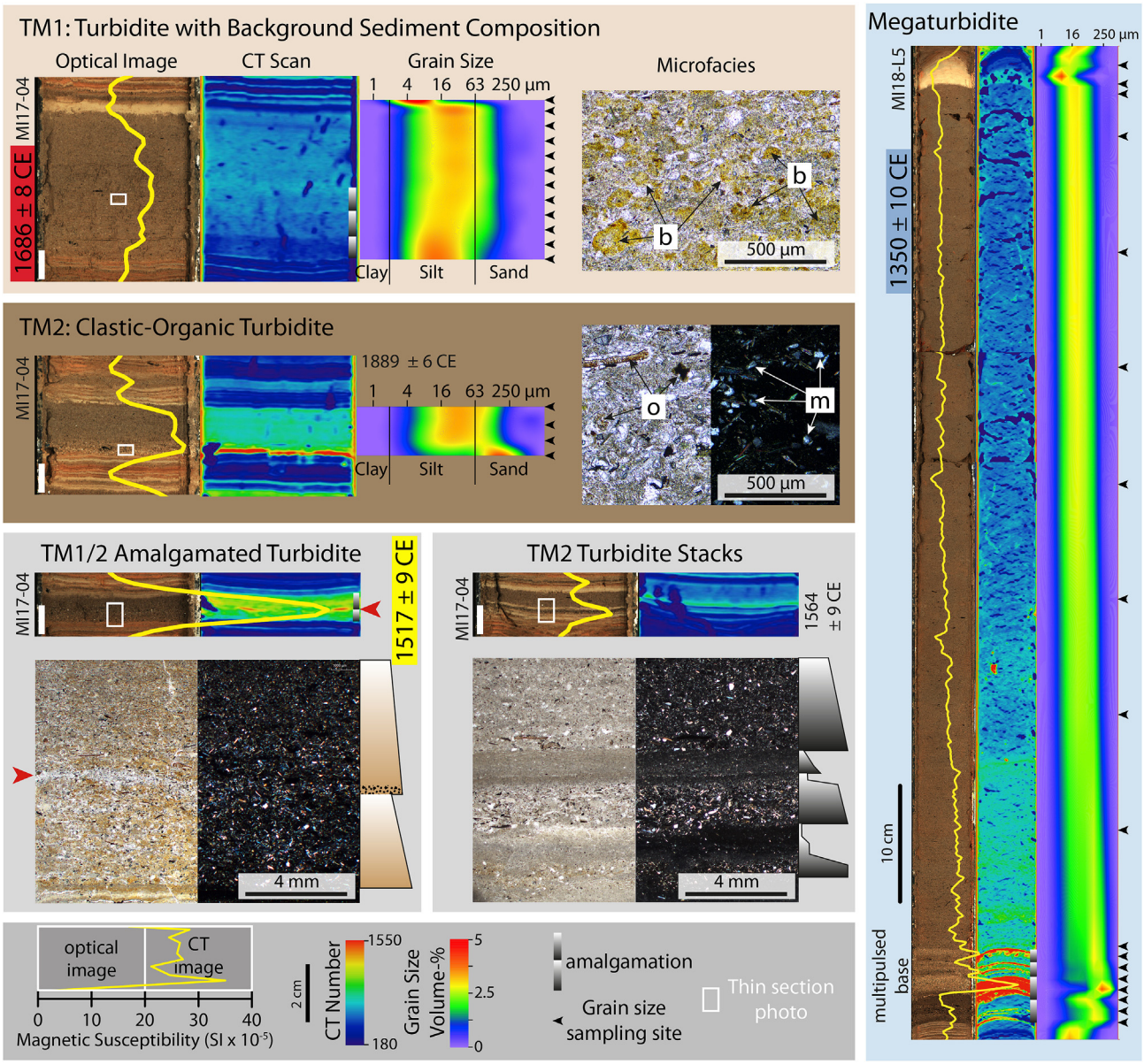

Fig. 7. Types of turbidites in Millstätter See. Based on their composition and thickness, we discriminate four main types of turbidites: turbidites largely consisting of background sediment patches (denoted as "b"; TM1), turbidites with high amounts of clastic minerogenic components ("m") and organic matter ("o"; TM2), and megaturbidites. Rarely, turbidites can also have a mixed composition between TM1s and TM2s, i.e. high content of clastic components with interspersed background sediment patches. Certain turbidites, such as the mixed turbidite dated to 1517 ± 9, show a distinct amalgamation pattern (red arrow). A common feature in the sediment cores of Millstätter See are clastic-organic turbidite stacks.

processes leading to TW2s and TM2s include (subaqueous) slope failures of alluvial fans and deltas, or debris flows and floods. Due to small and vegetated catchment areas and gentle topography, fluviatile sediment transport entering Wörthersee is small even during high runoff events. Moreover, sediment transport via the largest inflow (the Reifnitzbach, entering the eastern basin) is limited because an upstream lake (Keutschacher See) can act as a sediment trap. Small-scale TW2s (clastic-organic rich turbidites) are frequently present in front of inflows (e.g. in core WOER17-22; Fig. 5), indicating that minor floods only cause thin (<1 cm) turbidites in the record of Wörthersee. More prominent TW2s are therefore most likely related to the failure of subaqueous slopes within the influence of river inflows. In Millstätter See, we expect that prominent TM2s can also be caused by fluviatile processes, because the relatively large catchment area exhibits steep slopes of easily erodible mica schists and the sediment influx during heavy precipitation events is therefore potentially high. Analogous to hemipelagic slopes, alluvial fans and deltas tend to fail due to earthquake shaking (Moernaut, 2020), but also spontaneous collapses (Girardclos et al., 2007; Hilbe and Anselmetti, 2014) or flood-related failure (Vandekerkhove et al., 2020) has been reported in a few cases.

5.1.2. *Attributing event layers to historical earthquake events and assessing their imprint*

In lacustrine paleoseismic studies, seismic origin of turbidites and their causative landslides is often inferred via the synchronicity criterion, which is based on the assumption that simultaneous failure of several slopes in a lake requires a regional triggering mechanism, i.e. earthquake shaking (Hubert-Ferrari et al., 2020;

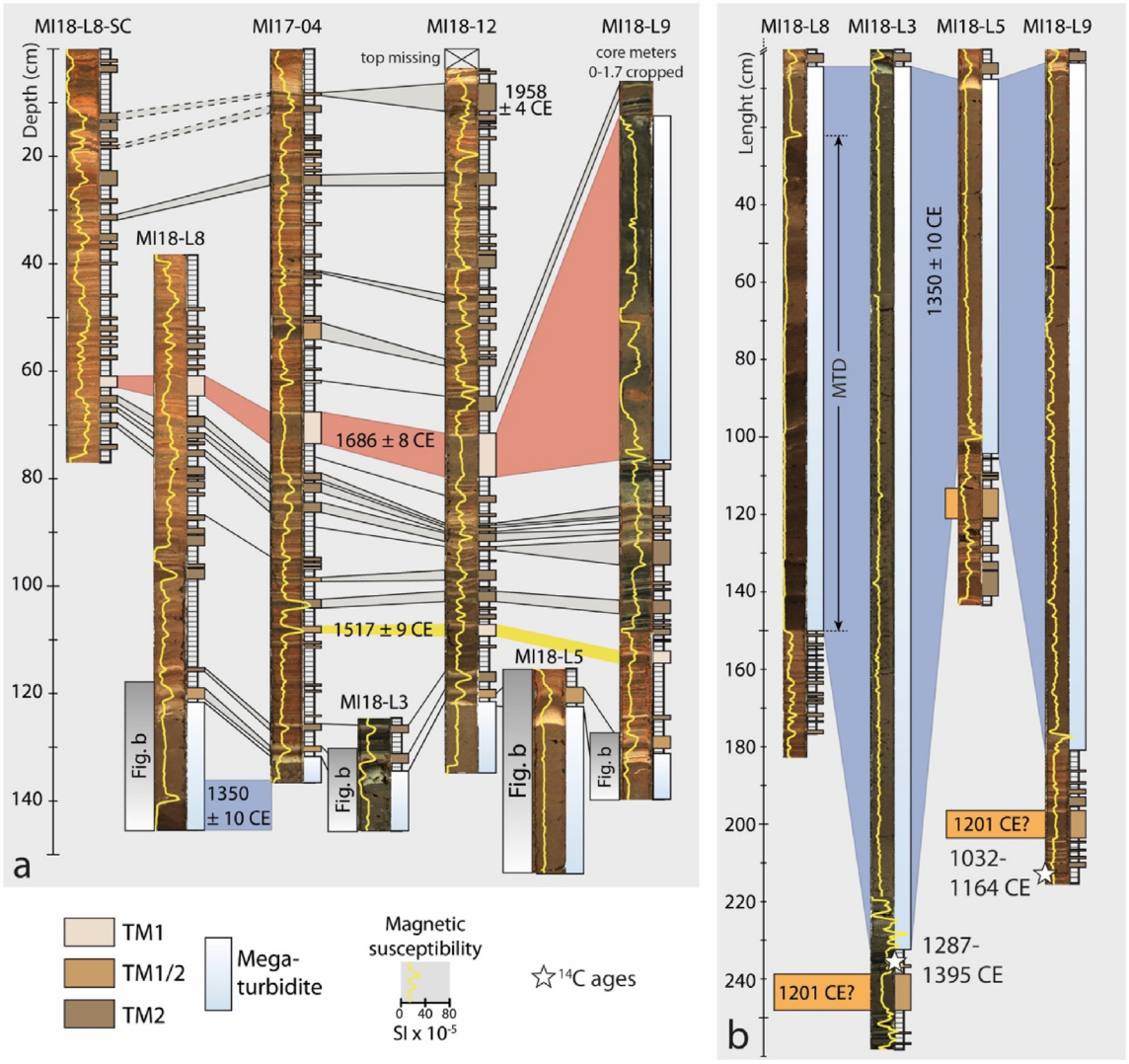

Fig. 8. Correlation of sediment cores from the four main basins of Millstätter See. **(a)** Correlation of the uppermost ~140 cm and correlation of short-to long cores. For core MI18-L9, the uppermost 1.7 m were cropped for reasons of visibility. The whole studied interval of core MI18-L9 as well its seismic-to-core-correlation is given in supplementary data 10. **(b)** In all lake basins, the event of 1350 ± 10 CE is recorded either as an MTD or a megaturbidite. Note that the depth-scale differs from Fig. 8a.

Oswald et al., 2021a; Praet et al., 2017). Synchronous landsliding can be archived in the sedimentary record as i) multiple MTDs on a single seismostratigraphic level (Schnellmann et al., 2002), ii) amalgamated turbidites (Van Daele et al., 2017) and iii) correlating turbidites in different lake basins or depositional areas (DA; e.g. Howarth et al., 2021; Moernaut et al., 2014). DAs are defined as physically connected areas in a lake where a similar earthquake imprint is expected (following Van Daele et al., 2015; see Fig. 9 and Fig. 10 for location of DAs).

In Wörthersee, the turbidites dated to 1976 ± 1, 1853 ± 6, 1704 ± 12, 1515 ± 16 and 1364 ± 22 are the only ones that can be traced over several depositional areas or even lake basins (Figs. 5 and 9). MTDs were mapped for all these events except for 1976 ± 1 CE. Furthermore, amalgamated turbidites are present for the events of 1853 ± 6, 1704 ± 12 and 1364 ± 22. The spatial distribution of turbidite thickness and grain-size of the event deposits further corroborates core-to-seismic correlation and proves the landslide origin of these turbidites: the further the turbidite is located from its causative landslide, the smaller the turbidite and its maximum grain-size.

In Millstätter See, many turbidites can be correlated across the depositional areas (Fig. 8). Here, the synchronicity criterion cannot be applied in a straightforward manner, because also a large-scale precipitation event along the north-eastern shore of Millstätter See might lead to the deposition of a TM2 in several depositional areas. To infer a seismic trigger of event deposits, it is therefore important to also take the associated mappable landslides and turbidite composition into account. Multiple MTDs are present for the events of 1958 ± 4, 1686 ± 8, 1517 ± 9, 1350 ± 10 and ~1350–1100 CE (Fig. 10). Amalgamated turbidites and/or turbidites with a lake-internal composition are present for the events of 1686 ± 8, 1517 ± 9, 1350 ± 10 and ~1350–1100 CE.

Based on their sedimentological characteristics, spatial distribution and the temporal correlation, the event deposits dated to 1976 ± 1, 1853 ± 6, 1704 ± December 1686 ± 8, 1515 ± 16/1517 ± 9 and 1364 ± 22/1350 ± 10 can be reliably attributed to the historical earthquakes of 1976, 1857, 1690, 1511 and 1348, respectively (Tables 2 and 3). Because of its lake-internal composition and multiple mapped MTDs, we attribute the less precisely dated turbidite of ~1350–1100 CE to the earthquake of 1201 CE. The event deposits dated to 1958 ± 4 CE in Millstätter See, which have a pure TM2 composition and are therefore distinctly different from the

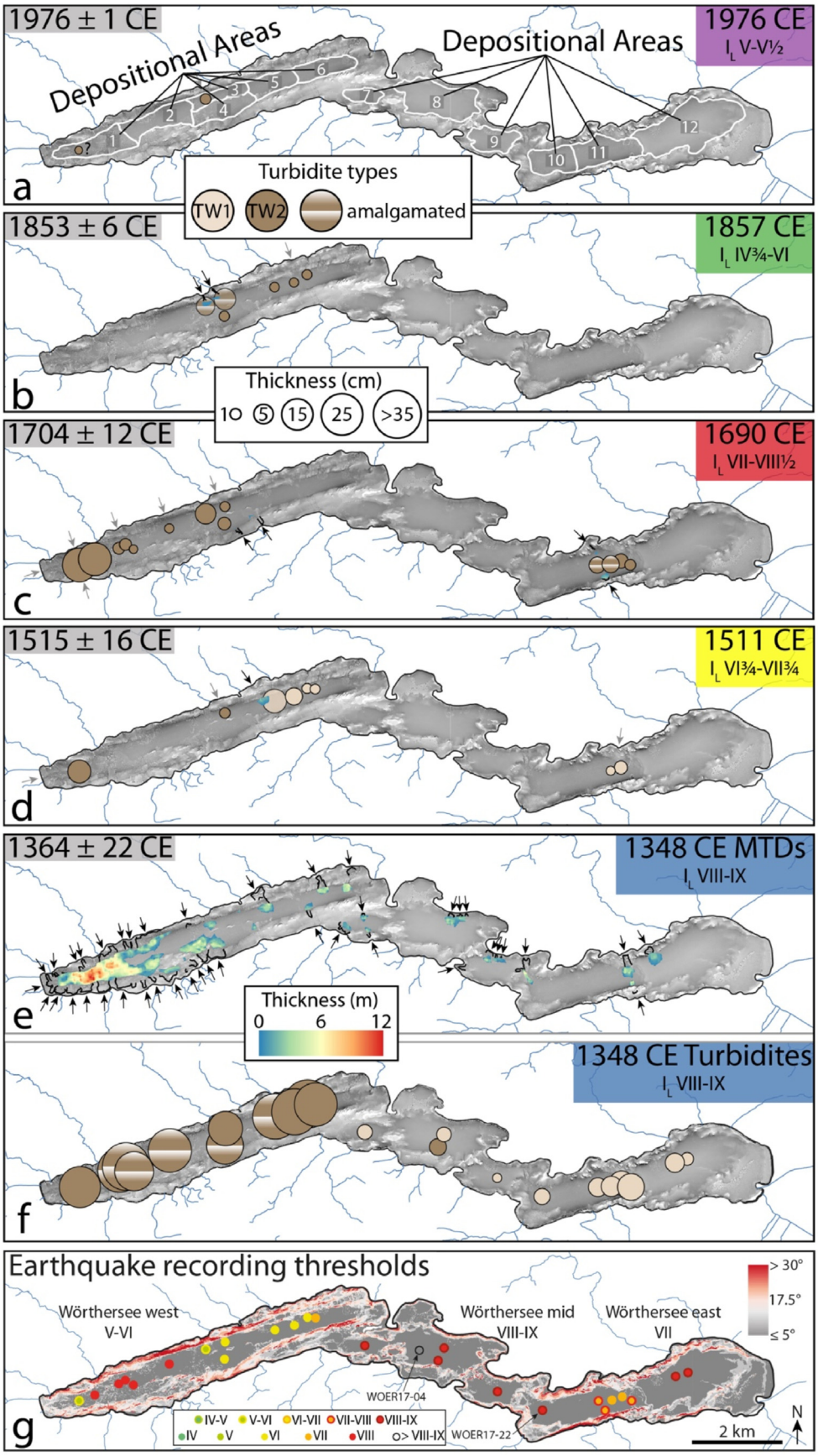

Fig. 9. Spatial imprint of synchronous event deposits in Wörthersee, corresponding to the main earthquakes, and site-specific earthquake-recording thresholds. Individual subaqueous slope failures are denoted by arrows. Grey arrows indicate slope failures that could not be mapped in the bathymetric or seismic data but are inferred from the presence of

turbidites related to earthquakes, are the result of debris flows and subsequent delta failures following intense precipitation (Schwarzl, 1971).

A detailed description of the earthquake imprints is given in supplementary data 11.

5.1.3. Challenges in assessing the lacustrine imprint of earthquakes

Especially in areas with multiple landsliding (e.g. in the westernmost part of Wörthersee), mapping of individual landslides is hampered due to limits in seismic penetration and overprinting of MTD evidence by subsequent events. Overprinting also applies to mapping of individual failure scars in the bathymetric map, for which we counted the number of failure scars that are separated by unfailed slope areas (Figs. 9 and 10). Therefore, an under- or overestimation of event volumes and number of slope failures may occur in certain lake areas. However, most of the mapped MTDs are clearly single landslide events and can be reliably mapped within the limits of seismic resolution.

Small errors are introduced into the varve record by missing, disturbed or overcounted varves. In Wörthersee, some lithofacies show very thin varves that can remain undetected. To evaluate and reduce varve counting uncertainties, independent and repeated varve counts on different cores were conducted. In Millstätter See, where sedimentation rates are generally high and varve preservation is exceptionally good, varve counting on a single core is sufficient to establish a precise age-depth-model. This age-depth model was projected to cores of different basins using the general patterns of turbidite deposition and background-sedimentation variations (whitish, diatom-rich layers). However, multiple flood-induced pulses in a single varve complicate identification of varve-year boundaries and could lead to an overestimation of the varve age. Therefore, the presented uncertainty on the varve chronologies (Figs. 3 and 6; Table 2) is a measure of the methodological precision and does not represent chronological accuracy. This could explain the minor offset between the age of the 1690 CE earthquake and the uncertainty range (1σ) of its corresponding varve age in Wörthersee (1704 ± 12 CE). The ages of all other historical earthquakes that were linked to turbidites fall within the 1σ uncertainty ranges of the varve ages.

5.2. Quantitative paleoseismology

5.2.1. Earthquake-recording thresholds and site-dependency

The main historical earthquakes of 1348 CE, 1511 CE and 1690 CE are recorded as multiple MTDs and turbidites in the sedimentary infill of both Wörthersee and Millstätter See (Tables 2 and 3). Depending on earthquake magnitude and epicentre distance to the lake, local seismic intensities at these lakes range between VI¾ to IX. In contrast, the 1857 CE and 1976 CE Friuli earthquakes, which exhibited seismic intensities of V-VI in the study area, are only recorded in the western basin of Wörthersee as rather thin and local turbidites.

From the spatial distribution of turbidites and MTDs triggered by the documented earthquakes, we derive site-specific earthquake-recording thresholds (EQRTs; Figs. 9g and 10g). For most of the coring sites, these thresholds are intrinsically consistent, meaning that if an earthquake exhibiting a certain local intensity is recorded, seismic shaking of higher intensities are recorded as well. Only in the deepest part of the Western basin in Wörthersee this does not hold true, as the 1511 CE event (intensity VI¾ - VII¾) is present in the sedimentary archive as a minor turbidite, but the 1690 CE event (intensity VII½ - VIII½) is absent. This suggests that the EQRT is an intensity range rather than a single value.

For deltaic slopes, the EQRT in the western basin of Wörthersee can be as low as V½, whereas for hemipelagic slopes, this threshold ranges between VI-VIII½ (Fig. 9g). In Millstätter See, turbidity currents on hemipelagic slopes are induced from intensity of VII onwards (Fig. 10g). Failure of deltaic slopes from intensities of V½ and of hemipelagic slopes from VI-VII onwards is in agreement with findings from multi-core studies of recent and historical earthquakes in Chile (Moernaut et al., 2014; Van Daele et al., 2015), Alaska (Van Daele et al., 2019), Switzerland (Monecke et al., 2004) and France (Wilhelm et al., 2016). However, the high threshold values (VIII-VIII½) in some areas of Wörthersee indicate the influence of parameters other than the sedimentation type (hemipelagic vs. alluvial) on the slopes.

Most of the high-threshold sites are situated in the relatively shallow (~40 m) basins of Wörthersee (Fig. 9g). Compared to the low-threshold sites in the deeper parts of Wörthersee, these basins are bordered by shorter slopes, while at the same time comprising a relatively extensive basin flat. The zone of possible sediment deposition after slope failures is thus high compared to the amount of potentially remobilized sediment. This leads to a diluting effect and could explain the absence of macroscopically detectable turbidites in the sedimentary records. Because of its slightly more distal position (Fig. 9g), coring site WOER17-04 is the only coring site in Wörthersee which does not contain traces of the 1348 CE event. There are also areas in the relatively deep westernmost part of Wörthersee which show high EQRTs. The slopes adjacent to these areas were almost completely stripped from their Holocene sediment drape during the 1348 CE event, leading to the exposure of more consolidated Late Glacial sedimentary sequences (Daxer et al., 2020). This reduces the amount of unconsolidated, potentially unstable sediment available for failure during the subsequent events of 1511 CE and 1690 CE and might lead to the high estimated EQRTs there. Furthermore, extensive landsliding (as observed in Wörthersee and Millstätter See during the 1348 CE earthquake) can lead to a complex lake-floor morphology, affecting turbidity current flow-paths and potentially hampering effective transport of sediment to the coring sites located close to the MTDs. This effect is most likely responsible for slightly higher EQRTs in the westernmost part of Wörthersee and the northeastern part of Millstätter See.

The lack of distinctively differing basin morphologies and basin depths in Millstätter See leads to a consistent overall EQRT (~VII), which is higher than the most sensitive sites in Wörthersee (V½ – VI). This difference might be due to higher slope gradients and hence lower slope sediment accumulation rates. Generally, slope angles above 20° are affected by rather continuous gravitational reworking and therefore little accumulation of slope sediments, as suggested by seismic-stratigraphic analysis in Swiss (Strasser et al., 2011) and Alaskan lakes (Praet et al., 2017). An indicator of this effect in this study is formed by the scarp height of slope failures triggered by the 1348 CE earthquake, which are believed to have initiated near the Holocene-Late Glacial sediment boundary (Daxer et al., 2020). Scarp heights in Wörthersee are about 3–4 m, whereas those in Millstätter See are 2–3 m, potentially indicating thinner Holocene slope sequences.

turbidites in the sediment cores. **(a)** Imprint of the 1976 CE earthquake. Depositional areas are outlined in white. **(b)** Imprint of the 1857 CE earthquake. **(c)** Imprint of the 1690 CE earthquake. **(d)** Imprint of the 1511 CE earthquake. **(e)** MTDs caused by the 1348 CE earthquake. **(f)** Turbidites related to the 1348 CE earthquake. **(g)** Site-specific earthquake-recording thresholds derived from the presence or absence of sedimentary imprints related to earthquakes. Between the subbasins, the "general" EQRTs differ strongly (from V-VI to VIII-IX), depending on the depth of the respective subbasin. One coring site (WOER17-04), situated in the central middle basin, did not record any of the historical earthquakes, indicating a very high EQRT.

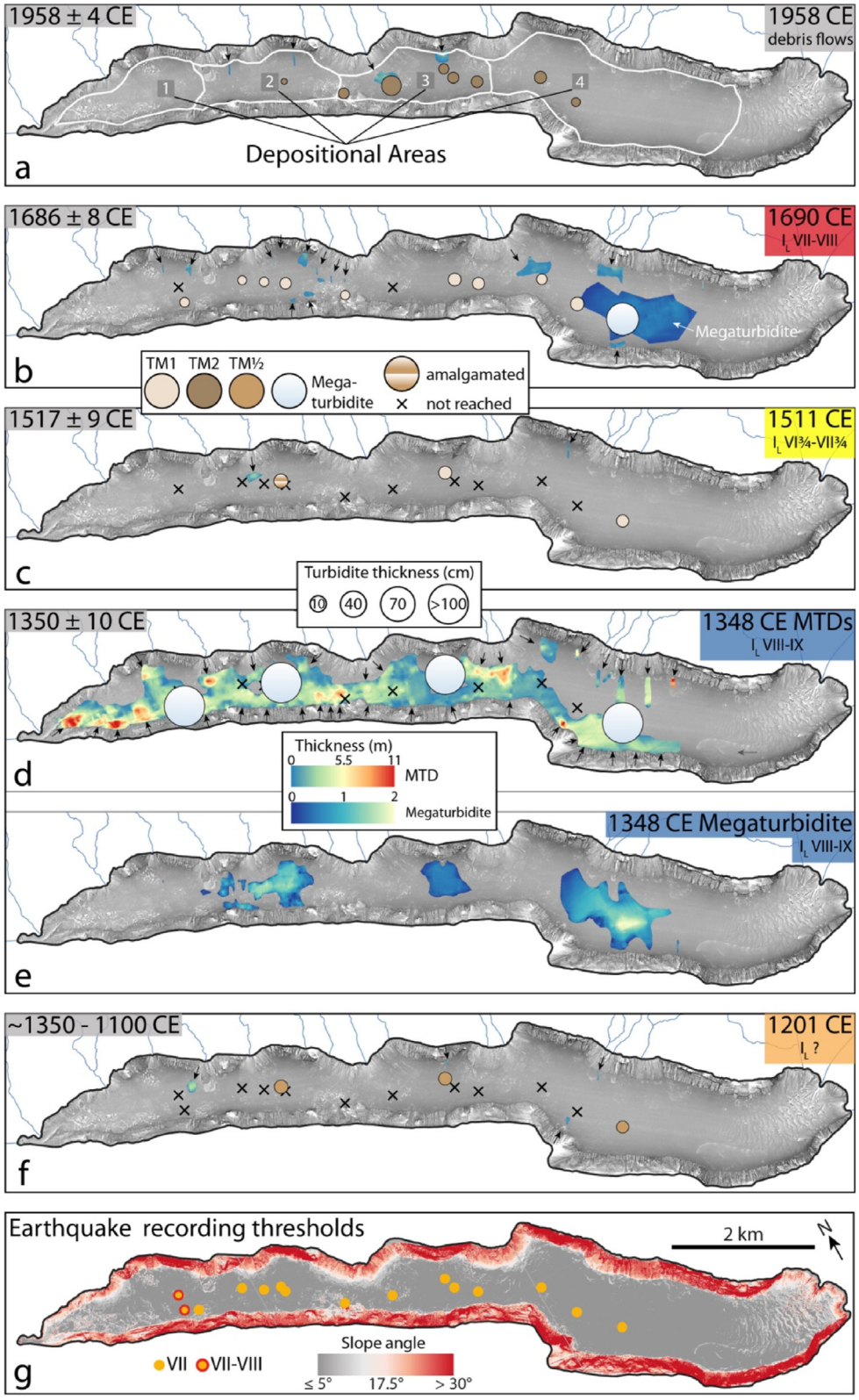

Fig. 10. Spatial imprint of synchronous event deposits for which MTDs were mapped and site-specific earthquake-recording thresholds in Millstätter See. Individual slope failures are denoted by arrows. Grey arrows indicate slope failures that could not be mapped in the bathymetric or seismic data but are inferred from the presence of turbidites in the sediment cores. Except for the event dated to 1958 ± 4 CE, which is related to debris flows, the event deposits of the other four stratigraphic levels are caused by historical earthquakes. **(a)** Imprint of the debris flows caused by an extreme precipitation event in 1958 (Schwarzl, 1971). Depositional areas are outlined in white. **(b)** Imprint of the 1690 CE earthquake. **(c)** Imprint of the 1511 CE earthquake. **(d)** MTDs and cored megaturbidites caused by the 1348 CE earthquake. **(e)** Thickness map of the megaturbidite caused by the 1348 CE earthquake, as obtained by seismic-stratigraphic mapping. **(f)** Imprint of the 1201 CE earthquake. **(g)** Site-specific earthquake-recording thresholds derived from the presence or absence of sedimentary imprints related to earthquakes. The EQRTs are consistent (VII) throughout the lake.

Table 2
Imprint of events that show simultaneous deposits in Wörthersee.

Age of event (CE ± error)	Corresponding seismic event horizon	# of mappable MTDs	MTD Volume (10^3 m^3)	DAs showing an imprint	Turbidites with predominantly lake internal composition	Amalgamated turbidites	Mega-turbidites	Cumulative turbidite thickness (cm)	Attributed historical earthquake
1976 ± 1	**-**	**0**		**1–2/12**	**No**	**No**	**No**	**1.0**	**1976 CE**
1853 ± 6	**EH-B**	**2**	**8.2**	**3/12**	**No**	**Yes**	**No**	**6.6**	**1857 CE**
1704 ± 12	**EH-C**	**4**	**21**	**5/12**	**No**	**Yes**	**No**	**20.5**	**1690 CE**
1515 ± 16	**EH-D**	**1**	**33.3**	**5/12**	**Yes**	**No**	**No**	**12.1**	**1511 CE**
1364 ± 22	**EH-E**	**41**	**5590**	**12/12**	**Yes**	**Yes**	**Yes**	**173.1**	**1348 CE**

Table 3
Imprint of events that show simultaneous deposits in Millstätter See.

Age of event (CE ± error)	Corresponding seismic event horizon	# of mappable MTDs	MTD Volume (10^3 m^3)	DAs showing an imprint	Turbidites with predominantly lake internal composition	Amalgamated turbidites	Mega-turbidites	Cumulative turbidite thickness (cm)	Attributed historical earthquake
1958 ± 4	**EH-A**	**2–4**	**78.5**	**3/4**	**No**	**No**	**No**	**15.6**	**-**
1686 ± 8	**EH-B**	**14**	**83**	**4/4**	**Yes**	**Yes**	**Yes**	**81.8**	**1690 CE**
1517 ± 9	**EH-C**	**2**	**23.7**	**3/4**	**No**	**Yes**	**No**	**4.5**	**1511 CE**
1350 ± 10	**EH-D**	**36**	**8860**	**4/4**	**Yes**	**Yes**	**Yes**	**648.0**	**1348 CE**
~1350–1100	**EH-E**	**3**	**32.5**	**3/4**	**Yes**	**No**	**No**	**14.9**	**1201 CE**

5.2.2. Size-scaling and possible implementation in the ESI-07 scale

Strong seismic shaking (I_L > V) can lead to different earthquake environmental effects, e.g. surface ruptures, soil liquefaction, hydrogeological anomalies, tsunamis and gravitational mass movements (Michetti et al., 2007). The Environmental Seismic Intensity Scale (ESI-07; Michetti et al., 2007; Silva et al., 2015) integrates the environmental effects caused by an earthquake to estimate seismic intensities. This is especially useful for prehistorical earthquakes and for historical earthquakes in scarcely populated areas for which only a few damage reports exist. Onshore landslides, for which relationships between seismic shaking strength/magnitude and the number and volume of landslides have been established (Keefer, 1994, 2002), are extensively considered in the ESI-07. Lacustrine slope failures, on the other hand, are only vaguely mentioned. It is stated that subaquatic landslides "may be" triggered from intensity V onwards, become "significant" from VII, and occur "frequently" from VIII. A robust relationship between the strength of shaking and the "size" of subaquatic landslides, however, is not given.

5.2.2.1. Mass-transport deposits. Our data show that the number of mappable mass-transport deposits as well as the MTD volumes per event increase with seismic intensity (Fig. 11a and b) in both lakes, following exponential trends. Slight offsets from an "ideal" trend can be explained by factors discussed in section 5.1, e.g. limited seismic penetration/coverage, or overprinting by subsequent events. The higher number of MTDs and relatively large remobilized sediment volume during the 1857 CE earthquake in comparison with the 1511 and 1690 CE events in Wörthersee, for instance, is likely caused by an underestimation of MTDs triggered by the latter two earthquakes. Indeed, major turbidites in the very west of Wörthersee as well as in the Eastern basin hint at substantial sediment remobilization during 1511 and 1690 CE. However, no MTDs could be mapped in these areas because of the morphological complexity generated by large MTDs during the 1348 CE event.

No size-scaling relationships for MTDs have been proposed yet in the subaqueous realm. One of the reasons for this is that the size and extent of translational failures on sublacustrine sedimentary slopes is rather governed by preconditioning factors instead of the intensity of the triggering mechanism. These factors include slope gradient, the trend of undrained shear strength with depth (Sammartini et al., 2021), geotechnically "weak" layers (Gatter et al., 2021) and frontal/lateral buttressing of slope sediments. Moreover, it must be taken into account that, after a landsliding event, a slope segment needs considerable time to recharge with soft sediments to generate the next translational slope failure. Therefore, for instance in Lake Lucerne, quantitative constraints on ground motion were obtained by basin-wide slope stability evaluations over the depositional history of the slopes (Strasser et al., 2011), but not by comparing the number and volume of MTDs. Despite the influence of several potential preconditioning factors, our Carinthian lake data show the high potential for MTD number and volume as a relative proxy for seismic shaking strength. This means that quantitative MTD paleoseismology is feasible if a very dense grid of high-resolution seismic profiles is acquired and ground-truthed by dated sediment cores.

5.2.2.2. Turbidites. In both Wörthersee and Millstätter See, the number of DAs in which an earthquake is recorded as a turbidite follows a linear trend with intensity. From intensities of VII½ (Millstättersee) or VIII (Wörthersee) onwards, a seismo-turbidite in every depositional area (= 100%) can be expected. This is in accordance with findings in Chile where a 100% turbidite presence is reached at intensity ~ VII½ (Van Daele et al., 2015), despite the very different seismotectonic and sedimentary settings. To consider variations in turbidite thickness, we summed up the mean turbidite thickness for all DAs and normalized this cumulative turbidite thickness (CTT) to the 1348 CE event (100%). Our data shows that the normalized CCT increases exponentially with seismic intensity, highlighting the outstanding imprint of the 1348 CE earthquake. This is especially apparent in the western basin of Wörthersee, where the 1348 CE megaturbidite leads to a very high CCT and a comparably low R^2 of 0.79. In the eastern basin, however, the exponential relationship fits perfectly (R^2 = 0.99).

5.3. Implications for (alpine) lake paleoseismology

5.3.1. Sensitivity of lacustrine paleoseismic records

For Alpine lakes, the ESTI (Earthquake sensitivity threshold index) method has been developed to quantify and compare the sensitivity of small lakes to record seismic shaking (Wilhelm et al., 2016). The ESTI is based on the epicentral intensity of earthquakes

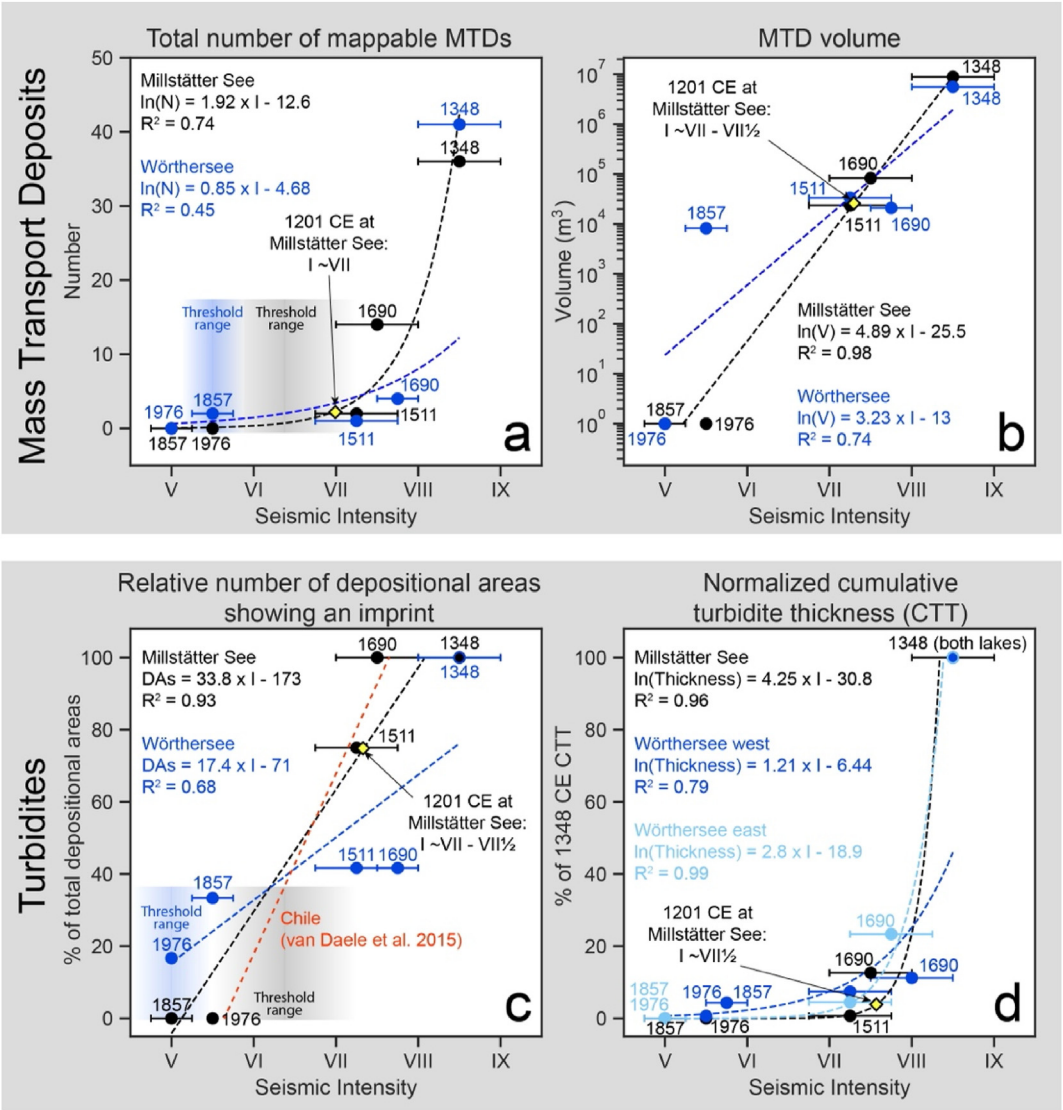

Fig. 11. Size-scaling relationships of earthquake imprint vs. seismic intensity. **(a)** Seismic intensity vs. total number of mappable MTDs (in bathymetric data and/or seismic data). The total number of mappable MTDs increases with seismic intensity. **(b)** Seismic intensity vs. MTD volume. The volume of remobilized sediment increases exponentially with seismic intensity. **(c)** Seismic intensity vs. relative number of depositional areas in a lake that record an earthquake (cf. Tables 2 and 3). The higher the seismic intensity, the more depositional areas show an earthquake imprint. From intensities ~ VII½ to VIII, seismic shaking is recorded in all areas. This agrees with findings from Chile (dashed red line; Van Daele et al., 2015). **(d)** Seismic intensity vs. normalized cumulative turbidite thickness (= the cumulated mean turbidite thicknesses per depositional area, normalized to the thickness of the AD1348 (mega-)turbidite). Cumulative turbidite thickness increases exponentially with seismic intensity. (For interpretation of the references to colour in this figure legend, the reader is referred to the Web version of this article.)

and their (non-)recording in a lake located at a certain distance from the epicentre. The ESTI is defined as the inverse of the intersection of a threshold line, separating recorded from non-recorded earthquakes, with the intensity axis at 10 km from the lake (Wilhelm et al., 2016). Lakes exhibiting a higher sensitivity to record earthquakes therefore are assigned higher ESTI-values. To aid comparability, we calculated the ESTI values of Wörthersee and Millstätter See using the same sensitivity threshold slope (0.13) as previous authors (Rapuc et al., 2018; Wilhelm et al., 2016, Fig. 12). For Millstätter See as well as the western and the eastern basin of Wörthersee, the ESTI is rather similar (~0.137–0.14). In the middle basin of Wörthersee, which is characterized by a high EQRT, the ESTI is lower (~0.13).

Based on compilations of lacustrine records from Alpine lakes, it is proposed that sedimentation rate is the main controlling factor for the sensitivity of lake sediments to record seismic shaking (Fig. 12b; Rapuc et al., 2018; Wilhelm et al., 2016). When sedimentation rate increases from ~0.25 mm/yr to ~2 mm/yr, the ESTI increases from ~0.12 to ~0.19 for lakes in different Alpine settings. The ESTI values for all depositional areas in our two studied lakes show that the Wörthersee DAs follow the general trend. This implies that, in addition to the potential influence of slope gradient, slope length and preceding large-scale mass movements (Section 5.2.1), also lake-internal variation in sedimentation rate is a controlling factor on the sensitivity of different depositional areas to record earthquake shaking. However, it should be noted that short-term fluctuations in sedimentation rate, as seen in Wörthersee and Millstätter See, do not influence the likelihood of subaqueous slope failures, because the failure plane typically lies in several metres sediment depth (Daxer et al., 2020; Strasser et al., 2007). This is evidenced by the minor imprint of the 1976 CE earthquake in Wörthersee, which occurred during an interval of relatively high

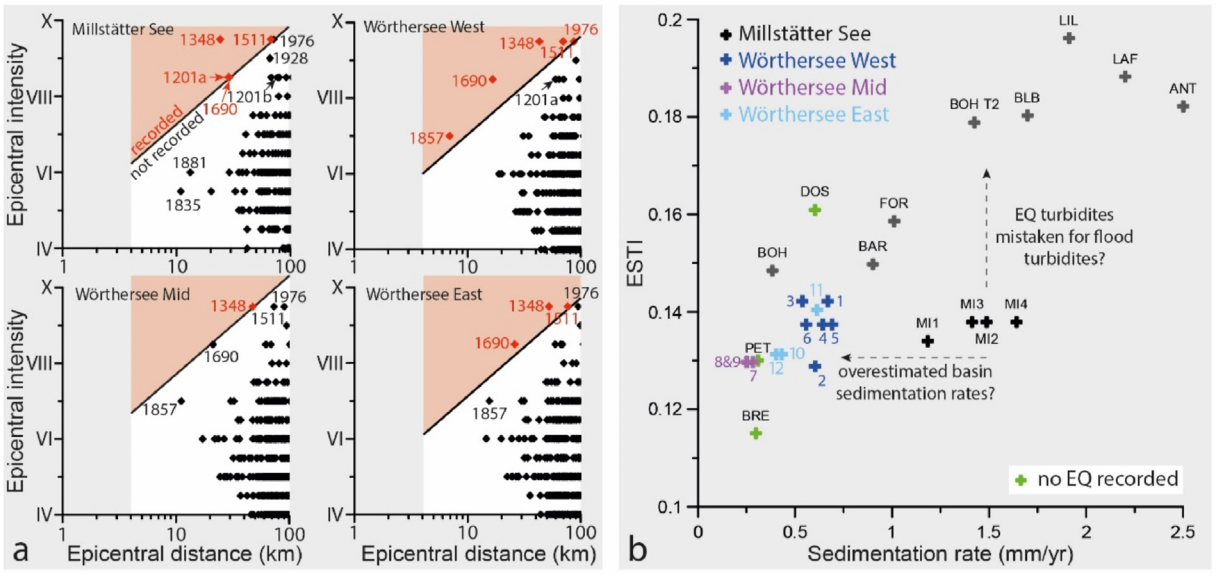

Fig. 12. Earthquake sensitivity threshold index (ESTI) calculations for Millstätter See and the three Wörthersee basins and their comparison to other lakes in the European Alps (Rapuc et al., 2018; Wilhelm et al., 2016). **(a)** Epicentral distance vs. epicentral intensity of historically and instrumentally recorded earthquakes as given in the SHEEC (Grünthal et al., 2013; Stucchi et al., 2013). The black line denotes the empirical limit separating recorded earthquakes (red diamonds) from earthquakes that are not recorded in the sedimentary records (black diamonds). For comparability, the "slope" of the threshold line (a in $y = a*ln(x) + b$) was defined as 1.13, as in the previous studies of Wilhelm et al. (2016) and Rapuc et al. (2018). The ESTI is defined as the inverse of intercept of the threshold line with the y-axis at 10 km epicentral distance. **(b)** Mean background sedimentation rates vs. ESTI-values. We compared the depositional areas of Wörthersee and Millstätter See with data from Alpine lakes.

sedimentation rates. In settings where seismo-turbidites result from surficial sediment remobilization (Moernaut et al., 2017; Molenaar et al., 2021) rather than MTDs, however, also short-term fluctuations of sedimentation rate might affect earthquake sensitivity.

In contrast to Wörthersee, the four DAs in Millstätter See are clearly offset from the general Alpine-wide trend (Fig. 12b). Even though the sedimentation rate in Millstätter See is rather high, its sensitivity remains much lower than the expected value. A possible explanation is related to our observational limit for detecting and identifying earthquake-induced turbidites in this lake. It cannot be excluded that relatively weak seismic shaking (V½ – VI½) may have destabilized deltaic slopes and left hemipelagic slopes intact, as the latter are less sensitive to seismic shaking (see section 5.2.1). Such seismo-turbidites with deltaic origin may be mistakenly identified as flood-related turbidites because their lithological composition can be very similar. Accordingly, the real ESTI-value of Millstätter See might be higher and fall closer to the expected trend. An alternative explanation for the outlying ESTI values might be an overestimation of sedimentation rates due to frequent small-scale (<1 mm) flood deposits, which are included in the "event-free" age model. Moreover, the presented sedimentation rates on the compilation of ESTIs concern core sites in the depositional basins, whereas seismically induced turbidity currents initiate on sedimentary slopes. There can be a large discrepancy between basin and slope sedimentation rates, especially when slope gradients are high (>20°) and the sedimentation is driven by underflows due to high discharge events. This is the case for Millstätter See, where slope accumulation rates might be very low (see Section 5.2.1). Future research should therefore focus also on documenting slope sedimentation rates to better understand earthquake-recording sensitivity of lake records.

5.3.2. *The 1201 CE event: application of size-scaling and considerations on epicentral location*

For the poorly documented historical 1201 CE earthquake, we apply our inferred size-scaling relationships to obtain an IDP for the location of Millstätter See (Fig. 11). Application of MTD number and MTD volume gives seismic intensities of ~VII and ~VII-VII½, respectively. This agrees with the values of turbidite-scaling relationships (~VII-VII½ for relative number of depositional areas and ~VII½ for normalized cumulative turbidite thickness). The 1348 CE earthquake caused extensive slope failures throughout the lake and therefore potentially led to an underrepresentation of the subsequent events (1511 and 1690 CE) in the sedimentary archive, affecting the derived size-scaling relations. Therefore, we consider the obtained intensity value of VII-VII½ for the 1201 CE event rather a maximum estimate. It is considerably lower than an IDP value (VIII to IX) about 75 km north-east of Millstätter See documented by Alexandre (1990), which would support the proposed epicentre location in that area. However, critical re-examination of historical sources questions the IDP values and relocates these together with the epicentre location about 60 km towards the west (Katschberg region), which is much closer to Millstätter See. Following this idea and considering our IDP value of VII-VII½ at Millstätter See, this would imply a magnitude of ~6.4 (considering the Austrian IPE; Papí Isaba et al., 2020) for the oldest historically documented earthquake in Austria, which is slightly higher than the magnitude derived by historical seismology (M_L ~6.1; ZAMG, 2021). For an alternative perspective, we used the ESTI approach (Fig. 12), where we compare the results of applying both epicentral locations. Together with the inferred positive sedimentary evidence at Millstätter See, the assumption of an epicentral intensity of VIII – IX implies that the datapoint must fall left of the threshold line, and thus the lake-to-epicentral distance should be less than 30 km. In

conclusion, both approaches based on the sedimentary archive of Millstätter See supports the epicentral location proposed by ZAMG (2021) close to the Katschberg region (Fig. 1).

6. Conclusions

By integration of multibeam bathymetry, high-resolution seismic reflection profiling and multiple precisely dated sediment cores in Millstätter See and Wörthersee, we tracked the sedimentary imprint of five historically documented earthquakes that affected Carinthia. This imprint consists of multiple coeval MTDs and associated (mega-)turbidites and was mapped in high spatio-temporal resolution throughout the basins. Because the macroseismic intensities of these earthquakes are well documented and the earthquakes are well spaced in time, we were able to i) confidently link sedimentary event deposits with their causative earthquakes and ii) evaluate the lacustrine sedimentary imprint related to different seismic intensities. We present the following conclusions:

- Based on the presence or absence of sedimentary imprints for specific earthquakes, site-specific intensity thresholds can be obtained and can range between V½ and VIII½. These threshold values can vary depending on the core location as these principally relate to composition, length and gradient of the slopes and the transport distance to the core sites. This implies that multi-threshold paleoseismic records can be obtained by long coring of multiple sites in a single basin. However, previous extensive landslide events (such as in 1348 CE) and their effects on basin morphology and slope sequences may locally influence these threshold values.
- Size-scaling relationships can exist between seismic intensity and i) MTD number, ii) MTD volume, iii) relative turbidite presence and iv) cumulative turbidite thickness. Overall, the best fit was found for exponential regressions, except for a linear fit for the relative turbidite presence. For turbidite records, similar relationships were found in Chilean lakes, whereas this study presents the first scaling relationships related to subaqueous mass-transport deposits.
- As proposed in previous studies, sedimentation rate can be considered a key parameter controlling the recharging and failure sensitivity of sublacustrine slopes. Therefore, it is crucial to document sedimentation rates on slopes instead of the common practice of inferring these from core sites in depositional basins. This is highlighted by the data from the steep-sloped Millstätter See, where contrasting rates were identified and therefore its data did not fit well into an Alpine-wide relation of earthquake-sensitivity of lakes compared to their sedimentation rates.
- Application of the obtained size-scaling relationships and sensitivity evaluations on the poorly documented historical 1201 CE earthquake sheds new light on the earthquake source parameters. In combination with historical documentation, our sedimentary data suggests a magnitude of about 6.4 and an epicentre closer than 30 km to Millstätter See, which would fit to the Katschberg region.

Author contributions

Christoph Daxer: Conceived and designed the analysis, Collected the data, Performed the analysis, Wrote the paper. Marcel Ortler: Collected the data, Contributed data or analysis tools. Stefano C. Fabbri: Collected the data, Contributed data or analysis tools. Michael Hilbe: Collected the data, Contributed data or analysis tools. Irka Hajdas: Contributed data or analysis tools. Natalie Dubois: Contributed data or analysis tools. Thomas Piechl: Contributed data or analysis tools. Christa Hammerl: Collected the data, Contributed data or analysis tools. Michael Strasser: Conceived and designed the analysis, Collected the data, Contributed data or analysis tools. Jasper Moernaut: Conceived and designed the analysis, Collected the data, Contributed data or analysis tools.

Data availability

The Austrian earthquake catalogue is available from the ZAMG (Central Institute for Meteorology and Geodynamics, Austria) upon reasonable request. Seismic and core data from Wörthersee are available on zenodo (https://doi.org/10.5281/zenodo.5875576), as are the seismic and core data (https://doi.org/10.5281/zenodo.5875911) and the bathymetric data (https://doi.org/10.5281/zenodo.5875923) from Millstätter See.

Declaration of competing interest

The authors declare that they have no known competing financial interests or personal relationships that could have appeared to influence the work reported in this paper.

Acknowledgments

This project was funded by the Austrian Science Fund (FWF), project number P30285−N34, the Austrian Academy of Sciences project “S4SLIDE-Austria” and the European Regional Development Fund Interreg V-A Italy-Austria 2014−2020 (project ITAT3016-Armonia). Christoph Daxer acknowledges financial support from a research grant from the University of Innsbruck (Exzellenzstipendium für Doktoratskollegs). We thank ETH Zurich for access to the Kullenberg coring system and platform and we are very grateful to all the people who helped carrying out fieldwork and retrieving Kullenberg-cores on Wörthersee and Millstätter See: Jyh-Jaan Steven Huang, Ariana Molenaar, Patrick Ostwald, Remo Röthlin and Reto Seifert. The Research Department for Limnology (ILIM, Mondsee) and Hannes Höllerer are thanked for providing the research vessel Luna and logistical help, as is the Carinthian Institute of Lake Research (KIS). The multibeam data of Wörthersee was kindly provided by the state of Carinthia (Land Kärnten, Abteilung Umwelt, Energie und Naturschutz). Further acknowledged is Pascal Rünzi for both radionuclide dating and helping during field work. We are very grateful to Markus Erhardt, Gerald Degenhart and Wolfgang Recheis for the use of the medical CT scanner at the Medical University of Innsbruck and to Julia Wallraf for preparing the numerous thin sections. IHS Markit is thanked for its educational grant program providing the KINGDOM seismic interpretation software. We thank an anonymous reviewer for their constructive comments.

Appendix A. Supplementary data

Supplementary data to this article can be found online at https://doi.org/10.1016/j.quascirev.2022.107497.

References

Albarello, D., D'Amico, V., 2004. Attenuation relationship of macroseismic intensity in Italy for probabilistic seismic hazard assessment. Boll. di Geofis. Teor. ed Appl. 45, 271−284.
Alexandre, P., 1990. Les Séismes en Europe occidentale de 394 à 1259: Nouveau catalogue critique. Observatoire Royal de Belqique, Bruxelles.
Ambraseys, N.N., 1976. The Gemona di Friuli earthquake of 6 may 1976. Part II. In:

Promotion of the Study of Natural Hazards of Geophysical Origin. UNESCO, Paris, pp. 81–85.
Anderle, N., 1977. Geologische Karte der Republik Österreich 1:50000. Villach-Assling, pp. 201–210.
Archer, C., Noble, P., Rosen, M.R., Sagnotti, L., Florindo, F., Mensing, S., Piovesan, G., Michetti, A.M., 2019. Lakes as paleoseismic records in a seismically-active, low-relief area (Rieti Basin, central Italy). Quat. Sci. Rev. 211, 186–207. https://doi.org/10.1016/j.quascirev.2019.03.004.
Avşar, U., Hubert-Ferrari, A., De Batist, M., Lepoint, G., Schmidt, S., Fagel, N., 2014. Seismically-triggered organic-rich layers in recent sediments from Göllüköy lake (north Anatolian fault, Turkey). Quat. Sci. Rev. 103, 67–80. https://doi.org/10.1016/j.quascirev.2014.08.020.
Bouma, A.H., 1987. Megaturbidite: an acceptable term? Geo Mar. Lett. 7, 63–67. https://doi.org/10.1007/BF02237985.
Brückl, E., Behm, M., Decker, K., Grad, M., Guterch, A., Keller, G.R., Thybo, H., 2010. Crustal structure and active tectonics in the Eastern Alps. Tectonics 29. https://doi.org/10.1029/2009tc002491.
Bruel, R., Sabatier, P., 2020. serac: a R package for ShortlivEd RAdionuclide chronology of recent sediment cores. J. Environ. Radioact. 225, 106449. https://doi.org/10.1016/j.jenvrad.2020.106449.
Camassi, R., Caracciolo, C.H., Castelli, V., Slejko, D., 2011. The 1511 Eastern Alps earthquakes: a critical update and comparison of existing macroseismic datasets. J. Seismol. 15, 191–213. https://doi.org/10.1007/s10950-010-9220-9.
Castellarin, A., Cantelli, L., 2000. Neo-alpine evolution of the southern eastern Alps. J. Geodyn. 30, 251–274. https://doi.org/10.1016/S0264-3707(99)00036-8.
Conrad, O., Bechtel, B., Bock, M., Dietrich, H., Fischer, E., Gerlitz, L., Wehberg, J., Wichmann, V., Böhner, J., 2015. System for automated geoscientific analyses (SAGA) v. 2.1.4. Geosci. Model Dev 8, 1991–2007. https://doi.org/10.5194/gmd-8-1991-2015.
Daxer, C., Sammartini, M., Molenaar, A., Piechl, T., Strasser, M., Moernaut, J., 2020. Morphology and spatio-temporal distribution of lacustrine mass-transport deposits in Wörthersee, Eastern Alps, Austria. Geol. Soc. London, Spec. Publ. 500, 235–254. https://doi.org/10.1144/SP500-2019-179.
Delbrück, H., 2010. Drei Erdbeben. In: Neues Aus Alt-Villach. Jahrbuch Des Stadtmuseums. https://doi.org/10.1524/hzhz.1890.65.jg.465.
Eder, N., Neubauer, F., 2000. On the edge of the extruding wedge: neogene kinematics and geomorphology along the southern Niedere Tauern, Eastern Alps. Eclogae Geol. Helv. 93, 81–92.
Fäh, D., Giardini, D., Kästli, P., Deichmann, N., Gisler, M., Schwarz-Zanetti, G., Alvarez-Rubio, S., Sellami, S., Edwards, B., Allmann, B., 2011. ECOS-09 earthquake catalogue of Switzerland release 2011 report and database. In: Public Catalogue, 17. 4. 2011. Swiss Seismological Service ETH Zurich, Risk, pp. 1–42.
Findenegg, I., 1933. Alpenseen ohne Vollzirkulation. Int. Rev. der gesamten Hydrobiol. und Hydrogr. 28, 295–311. https://doi.org/10.1002/iroh.19330280309.
Gatter, R., Clare, M.A., Kuhlmann, J., Huhn, K., 2021. Characterisation of weak layers, physical controls on their global distribution and their role in submarine landslide formation. Earth-Science Reviews 223. https://doi.org/10.1016/j.earscirev.2021.103845.
Girardclos, S., Schmidt, O.T., Sturm, M., Ariztegui, D., Pugin, A., Anselmetti, F.S., 2007. The 1996 AD delta collapse and large turbidite in Lake Brienz. Mar. Geol. https://doi.org/10.1016/j.margeo.2007.03.011.
Grünthal, G., Musson, R.M.W., Schwarz, J., Stucchi, M., 1998. European macroseismic scale 1998 (EMS-98). Cah. du Cent. Eur. Géodynamique Séismologie 15, 101. https://doi.org/10.2312/ems-98.full.en.
Grünthal, G., Wahlström, R., Stromeyer, D., 2013. The SHARE European earthquake catalogue (SHEEC) for the time period 1900-2006 and its comparison to the European-Mediterranean earthquake catalogue (EMEC). J. Seismol. 17, 1339–1344. https://doi.org/10.1007/s10950-013-9379-y.
Guidoboni, E., Comastri, A., 2005. Catalogue of Earthquakes and Tsunamis in the Mediterranean Area from the 11th to the 15th Century. NGV-SGA, Bologna.
Guidoboni, E., Ferrari, G., Tarabusi, G., Sgattoni, G., Comastri, A., Mariotti, D., Ciuccarelli, C., Bianchi, M.G., Valensise, G., 2019. CFTI5Med, the new release of the catalogue of strong earthquakes in Italy and in the Mediterranean area. Sci. Data 6, 80. https://doi.org/10.1038/s41597-019-0091-9.
Hammerl, C., 2008. Studies on 1000-1750 earthquakes in Austria. NERIES NA4 Collab. Rep. 1–2.
Hammerl, C., 1995. Das Erdbeben vom 4. Mai 1201. Mitteilungen des Instituts für Österreichische Geschichtsforsch 103, 350–368.
Hammerl, C., 1994. The earthquake of January 25th, 1348, discussion of sources. Hist. Investig. Eur. Earthquakes. Mater. CEC Proj. "Review Hist. Seism. Eur. 2, 225–240.
Hibsch, C., Alvarado, A., Yepes, H., Perez, V.H., Sébrier, M., 1997. Holocene liquefaction and soft-sediment deformation in Quito (Ecuador): a paleoseismic history recorded in lacustrine sediments. J. Geodyn. 24, 259–280. https://doi.org/10.1016/s0264-3707(97)00010-0.
Hilbe, Michael, Anselmetti, Flavio, 2014. Signatures of slope failures and river-delta collapses in a perialpine lake (Lake Lucerne, Switzerland). Sedimentology (7), 1883–1907. https://doi.org/10.1111/sed.12120.
Homann, O., 1962. Die geologisch-petrographischen Verhältnisse im Raume Ossiachersee - Wörthersee (südlich Feldkirchen zwischen Klagenfurt und Villach). Jahrb. Geol. Bundesanst. 105, 243–272.
Howarth, J.D., Barth, N.C., Fitzsimons, S.J., Richards-Dinger, K., Clark, K.J., Biasi, G.P., Cochran, U.A., Langridge, R.M., Berryman, K.R., Sutherland, R., 2021. Spatio-temporal clustering of great earthquakes on a transform fault controlled by geometry. Nat. Geosci. https://doi.org/10.1038/s41561-021-00721-4.
Howarth, J.D., Fitzsimons, S.J., Norris, R.J., Langridge, R., Vandergoes, M.J., 2016. A 2000 yr rupture history for the Alpine fault derived from lake Ellery, south Island, New Zealand. Bull. Geol. Soc. Am. 128. https://doi.org/10.1130/B31300.1.
Hubert-Ferrari, Aurélia, Lamair, Laura, Hage, Sophie, Schmidt, Sabine, Cagatay, Namik, Avsar, Ulas, 2020. A 3800 yr paleoseismic record (Lake Hazar sediments, eastern Turkey): Implications for the East Anatolian Fault seismic cycle. Earth and Planetary Science Letters. https://doi.org/10.1016/j.epsl.2020.116152.
Kahler, F., 1962. Geologische Karte der Umgebung von Klagenfurt 1, 50000.
Kärntner Institut für Seenforschung, 1992. Kärntner Seenbericht 1992 – 60 Jahre Seenforschung, 30 Jahre Seenreinhaltung. Veröffentlichungen des Kärntner Instituts für Seenforsch. 7, 471.
Kastelic, V., Vrabec, M., Cunningham, D., Gosar, A., 2008. Neo-Alpine structural evolution and present-day tectonic activity of the eastern Southern Alps: the case of the Ravne Fault, NW Slovenia. J. Struct. Geol. 30, 963–975. https://doi.org/10.1016/j.jsg.2008.03.009.
Keefer, D.K., 2002. Investigating landslides caused by earthquakes – a historical review. Surv. Geophys. 23, 473–510. https://doi.org/10.1023/A:1021274710840.
Keefer, D.K., 1994. The importance of earthquake-induced landslides to long-term slope erosion and slope-failure hazards in seismically active regions. Geomorphology 10, 265–284. https://doi.org/10.1016/0169-555X(94)90021-3.
Kelts, K., Briegel, U., Ghilardi, K., Hsu, K., 1986. The limnogeology-ETH coring system. Swiss J. Hydrol. 48, 104–115. https://doi.org/10.1007/BF02544119.
Kremer, K., Wirth, S.B., Reusch, A., Fäh, D., Bellwald, B., Anselmetti, F.S., Girardclos, S., Strasser, M., 2017. Lake-sediment based paleoseismology: limitations and perspectives from the Swiss Alps. Quat. Sci. Rev. 168, 1–18. https://doi.org/10.1016/j.quascirev.2017.04.026.
Lamoureux, S.F., 1994. Embedding unfrozen lake sediments for thin section preparation. J. Paleolimnol. 10, 141–146. https://doi.org/10.1007/BF00682510.
Lu, Y., Wetzler, N., Waldmann, N., Agnon, A., Biasi, G.P., Marco, S., 2020. A 220,000-year-long continuous large earthquake record on a slow-slipping plate boundary. Sci. Adv. 6, 1–11. https://doi.org/10.1126/sciadv.aba4170.
Michetti, A.M., Esposito, E., Guerrieri, L., Porfido, S., Serva, L., Tatevossian, R., Vittori, E., Audemard, F.A., Azuma, T., Clague, J., Comerci, V., Gürpinar, A., McCalpin, J., Mohammadioun, B., Mörner, N.A., Ota, Y., Roghozin, E., 2007. Environmental seismic intensity scale - ESI 2007. In: Vittori, E., Guerrieri, L. (Eds.), Memorie Descrittive Della Carta Geologica d'Italia. Servizio Geologico d'Italia, Roma, pp. 7–54.
Moernaut, J., 2020. Time-dependent recurrence of strong earthquake shaking near plate boundaries: a lake sediment perspective. Earth Sci. Rev. 210, 103344. https://doi.org/10.1016/j.earscirev.2020.103344.
Moernaut, J., Daele, M. Van, Heirman, K., Fontijn, K., Strasser, M., Pino, M., Urrutia, R., De Batist, M., 2014. Lacustrine turbidites as a tool for quantitative earthquake reconstruction: new evidence for a variable rupture mode in south central Chile. J. Geophys. Res. Solid Earth 119, 1607–1633. https://doi.org/10.1002/2013JB010738.
Moernaut, J., Van Daele, M., Fontijn, K., Heirman, K., Kempf, P., Pino, M., Valdebenito, G., Urrutia, R., Strasser, M., De Batist, M., 2018. Larger earthquakes recur more periodically: new insights in the megathrust earthquake cycle from lacustrine turbidite records in south-central Chile. Earth Planet Sci. Lett. 481, 9–19. https://doi.org/10.1016/j.epsl.2017.10.016.
Moernaut, Jasper, Van Daele, Maarten, Strasser, Michael, Clare, Michael A., Heirman, Katrien, Viel, Matías, Cardenas, Javiera, Kilian, Rolf, Ladrón de Guevara, Bruno, Pino, Mario, Urrutia, Roberto, De Batist, Marc, 2017. Lacustrine turbidites produced by surficial slope sediment remobilization: A mechanism for continuous and sensitive turbidite paleoseismic records. Marine Geology 384, 159–176. https://doi.org/10.1016/j.margeo.2015.10.009.
Molenaar, A., Van Daele, M., Vandorpe, T., Degenhart, G., De Batist, M., Urrutia, R., Pino, M., Strasser, M., Moernaut, J., 2021. What controls the remobilization and deformation of surficial sediment by seismic shaking? Linking lacustrine slope stratigraphy to great earthquakes in South-Central Chile. Sedimentology. https://doi.org/10.1111/sed.12856.
Monecke, K., Anselmetti, F.S., Becker, A., Schnellmann, M., Sturm, M., Giardini, D., 2006. Earthquake-induced deformation structures in lake deposits: a Late Pleistocene to Holocene paleoseismic record for Central Switzerland. Eclogae Geol. Helv. 99, 343–362. https://doi.org/10.1007/s00015-006-1193-x.
Monecke, K., Anselmetti, F.S., Becker, A., Sturm, M., Giardini, D., 2004. The record of historic earthquakes in lake sediments of Central Switzerland. Tectonophysics 394, 21–40. https://doi.org/10.1016/j.tecto.2004.07.053.
Moulin, A., Benedetti, L., Rizza, M., Jamšek Rupnik, P., Gosar, A., Bourlès, D., Keddadouche, K., Aumaître, G., Arnold, M., Guillou, V., Ritz, J.F., 2016. The Dinaric fault system: large-scale structure, rates of slip, and Plio-Pleistocene evolution of the transpressive northeastern boundary of the Adria microplate. Tectonics 35, 2258–2292. https://doi.org/10.1002/2016TC004188.
Musson, R.M.W., Grünthal, G., Stucchi, M., 2010. The comparison of macroseismic intensity scales. J. Seismol. 14, 413–428. https://doi.org/10.1007/s10950-009-9172-0.
Oswald, P., Strasser, M., Hammerl, C., Moernaut, J., 2021. Seismic control of large prehistoric rockslides in the Eastern Alps. Nat. Commun. 12, 1059. https://doi.org/10.1038/s41467-021-21327-9.
Papí Isaba, M., Weginger, S., Apoloner, M., Jia, Y., Hausmann, H., 2020. Intensity prediction equation for Austria : applications and analysis. EGU Gen. Assem. 2020. https://doi.org/10.5194/egusphere-egu2020-7683.
Pasolini, C., Albarello, D., Gasperini, P., D'Amico, V., Lolli, B., 2008. The attenuation of

seismic intensity in Italy, Part II: modeling and validation. Bull. Seismol. Soc. Am. 98, 692–708. https://doi.org/10.1785/0120070021.
Peruzza, L., 1996. Attenuating intensities. Ann. Geofisc. https://doi.org/10.4401/ag-4037.
Pistotnik, J., Daurer, A., Schönlaub, H.P., Matura, A., Scharbert, S., Plöchinger, B., Beck-Mannagetta, P., Oberhauser, R., 1980. Die östlichen Zentralalpen (südlich der Hohen Tauern und östlich der Katschberg-Linie). In: Der Geologische Aufbau Österreichs. Springer Vienna, pp. 348–404. https://doi.org/10.1007/978-3-7091-3744-4_19.
Praet, N., Moernaut, J., Van Daele, M., Boes, E., Haeussler, P.J., Strupler, M., Schmidt, S., Loso, M.G., De Batist, M., 2017. Paleoseismic potential of sublacustrine landslide records in a high-seismicity setting (south-central Alaska). Mar. Geol. 384, 103–119. https://doi.org/10.1016/j.margeo.2016.05.004.
Priolo, E., Barnaba, C., Bernardi, P., Bernardis, G., Bragato, P.L., Bressan, G., Candido, M., Cazzador, E., Di Bartolomeo, P., Durì, G., Gentili, S., Govoni, A., Klinc, P., Kravanja, S., Laurenzano, G., Lovisa, L., Marotta, P., Michelini, A., Ponton, F., Restivo, A., Romanelli, M., Snidarcig, A., Urban, S., Vuan, A., Zuliani, D., 2005. Seismic monitoring in northeastern Italy: a ten-year experience. Seismol Res. Lett. 76, 446–454. https://doi.org/10.1785/gssrl.76.4.446.
QGIS Development Team, 2018. QGIS Geographic Information System.
Rapuc, W., Sabatier, P., Andrič, M., Crouzet, C., Arnaud, F., Chapron, E., Šmuc, A., Develle, A., Wilhelm, B., Demory, F., Reyss, J., Régnier, E., Daut, G., Von Grafenstein, U., 2018. 6600 years of earthquake record in the Julian Alps (lake Bohinj, Slovenia). Sedimentology 65, 1777–1799. https://doi.org/10.1111/sed.12446.
Ratschbacher, L., Frisch, W., Linzer, H.-G, Merle, O., 1991. Lateral extrusion in the eastern Alps, PArt 2: structural analysis. Tectonics 10, 257–271. https://doi.org/10.1029/90TC02623.
Reichmann, M., Fresner, R., Schulz, L., 2014. Meromixis an Kärntner seen. Denisia 33, 129–133.
Reimer, P.J., Austin, W.E.N., Bard, E., Bayliss, A., Blackwell, P.G., Bronk Ramsey, C., Butzin, M., Cheng, H., Edwards, R.L., Friedrich, M., Grootes, P.M., Guilderson, T.P., Hajdas, I., Heaton, T.J., Hogg, A.G., Hughen, K.A., Kromer, B., Manning, S.W., Muscheler, R., Palmer, J.G., Pearson, C., Van Der Plicht, J., Reimer, R.W., Richards, D.A., Scott, E.M., Southon, J.R., Turney, C.S.M., Wacker, L., Adolphi, F., Büntgen, U., Capano, M., Fahrni, S.M., Fogtmann-Schulz, A., Friedrich, R., Köhler, P., Kudsk, S., Miyake, F., Olsen, J., Reinig, F., Sakamoto, M., Sookdeo, A., Talamo, S., 2020. The IntCal20 northern Hemisphere radiocarbon age calibration curve (0-55 cal kBP). Radiocarbon 62, 725–757. https://doi.org/10.1017/RDC.2020.41.
Reinecker, J., Lenhardt, W.A., 1999. Present-day stress field and deformation in eastern Austria. Int. J. Earth Sci. 88, 532–550. https://doi.org/10.1007/s005310050283.
Reiter, F., Freudenthaler, C., Hausmann, H., Ortner, H., Lenhardt, W., Brandner, R., 2018. Active seismotectonic deformation in front of the Dolomites indenter, Eastern Alps. Tectonics 1–30. https://doi.org/10.1029/2017TC004867.
Reitner, J.M., 2007. Glacial dynamics at the beginning of Termination I in the Eastern Alps and their stratigraphic implications. Quat. Int. 164–165, 64–84. https://doi.org/10.1016/j.quaint.2006.12.016.
Reitner, J.M., 2005. Landschaftsentwicklung im Quartär. Arb. Tagg. Geol. B.-A. 2005 Gmünd, pp. 63–81.
Reitner, J.M., Ertl, V., Ortner, G., Mandler, H., 2005. Exkursion : Quartärgeologie Millstätter See – Unterdrautal. Arb. Tagg. Geol. B.-A. 227–231, 2005 Gmünd.
Sammartini, M., Moernaut, J., Anselmetti, F.S., Hilbe, M., Lindhorst, K., Praet, N., Strasser, M., 2019. An Atlas of mass-transport deposits in lakes. In: Ogata, K., Festa, A., Pini, G.A. (Eds.), Submarine Landslides: Subaqueous Mass Transport Deposits from Outcrops to Seismic Profiles. American Geophysical Union, pp. 201–226. https://doi.org/10.1002/9781119500513.ch13.
Sammartini, M., Moernaut, J., Kopf, A., Stegmann, S., Fabbri, S.C., Anselmetti, F.S., Strasser, M., 2021. Propagation of frontally confined subaqueous landslides: insights from combining geophysical, sedimentological, and geotechnical analysis. Sediment. Geol. 416, 105877. https://doi.org/10.1016/j.sedgeo.2021.105877.
Sampl, H., 1976. Das Limnische Ökosystem des Millstätter Sees in Kärnten in den Letzten 40 Jahren. In: Müller, P. (Ed.), Verhandlungen Der Gesellschaft Für Ökologie Wien 1975: 5. Jahresversammlung Vom 22. Bis 24. September 1975 in Wien. Springer Netherlands, Dordrecht, pp. 129–137. https://doi.org/10.1007/978-94-015-7168-5_20.
Sánchez, L., Völksen, C., Sokolov, A., Arenz, H., Seitz, F., 2018. Present-day surface deformation of the Alpine region inferred from geodetic techniques. Earth Syst. Sci. Data 10, 1503–1526. https://doi.org/10.5194/essd-10-1503-2018.
Schmid, S.M., Fügenschuh, B., Kissling, E., Schuster, R., 2004. Tectonic map and overall architecture of the Alpine orogen. Eclogae Geol. Helv. 97, 93–117. https://doi.org/10.1007/s00015-004-1113-x.
Schnellmann, M., Anselmetti, F.S., Giardini, D., Mckenzie, J.A., 2006. 15,000 Years of mass-movement history in Lake Lucerne: implications for seismic and tsunami hazards. Eclogae Geol. Helv. 99, 409–428. https://doi.org/10.1007/s00015-006-1196-7.
Schnellmann, M., Anselmetti, F.S., Giardini, D., McKenzie, J.A., Ward, S.N., 2002. Prehistoric earthquake history revealed by lacustrine slump deposits. Geology 30, 1131. https://doi.org/10.1130/0091-7613(2002)030<1131:PEHRBL>2.0.CO;2.
Schulz, L., Schönhuber, M., Santner, M., Swaton, T., 2008. Erhebung des Ist-Zustandes der Uferverbauung und Seeeinbauten des Wörthersees und des Millstätter Sees. Publ. des Kärntner Instituts für Seenforsch. 4, 1–13.
Schuster, R., Pestal, G., Reitner, J.M., 2006. Erläuterungen zu Blatt 182 Spittal an der Drau. Geologische Bundesanstalt, Wien.
Schwarzl, S., 1971. Charakteristische Hochwasserlagen im Alpenraum, pp. 87–104. Vienna.
Silva, P.G., Michetti, A.M., Guerrieri, L., 2015. Intensity scale ESI 2007 for assessing earthquake intensities. In: Beer, M., Kougioumtzoglou, I.A., Patelli, E., Au, S.-K. (Eds.), Encyclopedia of Earthquake Engineering. Springer Berlin Heidelberg, Berlin, Heidelberg, pp. 1–20. https://doi.org/10.1007/978-3-642-36197-5_31-1.
Stein, S., Liu, M., Camelbeeck, T., Merino, M., Landgraf, A., Hintersberger, E., KüBler, S., 2017. Challenges in assessing seismic hazard in intraplate Europe. Geol. Soc. Spec. Publ. 432, 13–28. https://doi.org/10.1144/SP432.7.
Strasser, M., Hilbe, M., Anselmetti, F.S., 2011. Mapping basin-wide subaquatic slope failure susceptibility as a tool to assess regional seismic and tsunami hazards. Mar. Geophys. Res. 32, 331–347. https://doi.org/10.1007/s11001-010-9100-2.
Strasser, M., Monecke, K., Schnellmann, M., Anselmetti, F.S., 2013. Lake sediments as natural seismographs: a compiled record of Late Quaternary earthquakes in Central Switzerland and its implication for Alpine deformation. Sedimentology 60, 319–341. https://doi.org/10.1111/sed.12003.
Strasser, Michael, Stegmann, Sylvia, Bussmann, Felix, Anselmetti, Flavio S., Rick, Beat, Kopf, Achim, 2007. Quantifying subaqueous slope stability during seismic shaking: Lake Lucerne as model for ocean margins. Marine Geology 240 (1–4), 77–97. https://doi.org/10.1016/j.margeo.2007.02.016.
Stucchi, M., Rovida, A., Gomez Capera, A.A., Alexandre, P., Camelbeeck, T., Demircioglu, M.B., Gasperini, P., Kouskouna, V., Musson, R.M.W., Radulian, M., Sesetyan, K., Vilanova, S., Baumont, D., Bungum, H., Fäh, D., Lenhardt, W., Makropoulos, K., Martinez Solares, J.M., Scotti, O., Živčić, M., Albini, P., Batllo, J., Papaioannou, C., Tatevossian, R., Locati, M., Meletti, C., Viganò, D., Giardini, D., 2013. The SHARE European earthquake catalogue (SHEEC) 1000–1899. J. Seismol. 17, 523–544. https://doi.org/10.1007/s10950-012-9335-2.
Tertulliani, A., Cecic, I., Meurers, R., Sovic, I., Kaiser, D., Grünthal, G., Pazdirkova, J., Sira, C., Guterch, B., Kysel, R., Camelbeeck, T., Lecocq, T., Szanyi, G., 2018. The 6 May 1976 Friuli earthquake : re-evaluating and consolidating transnational macroseismic data. Boll. di Geofis. Teor. ed Appl. 59, 417–444. https://doi.org/10.4430/bgta0234.
Toperczer, M., Trapp, E., 1950. Ein Beitrag zur Erdbebengeographie Österreichs nebst Erdbebenkatalog 1904–1948 und Chronik der Starkbeben. Mitteilungen der Erdbebenkommission 59.
Valero-Garcés, B., Morellón, M., Moreno, A., Corella, J.P., Martín-Puertas, C., Barreiro, F., Pérez, A., Giralt, S., Mata-Campo, M.P., 2014. Lacustrine carbonates of Iberian Karst lakes: sources, processes and depositional environments. Sediment. Geol. 299, 1–29. https://doi.org/10.1016/j.sedgeo.2013.10.007.
Van Daele, M., Haeussler, P.J., Witter, R.C., Praet, N., De Batist, M., 2019. The sedimentary record of the 2018 Anchorage earthquake in Eklutna Lake, Alaska: calibrating the lacustrine seismograph. Seismol Res. Lett. 91, 126–141. https://doi.org/10.1785/0220190204.
Van Daele, M., Meyer, I., Moernaut, J., De Decker, S., Verschuren, D., De Batist, M., 2017. A revised classification and terminology for stacked and amalgamated turbidites in environments dominated by (hemi)pelagic sedimentation. Sediment. Geol. 357, 72–82. https://doi.org/10.1016/j.sedgeo.2017.06.007.
Van Daele, M., Moernaut, J., Doom, L., Boes, E., Fontijn, K., Heirman, K., Vandoorne, W., Hebbeln, D., Pino, M., Urrutia, R., Brümmer, R., De Batist, M., 2015. A comparison of the sedimentary records of the 1960 and 2010 great Chilean earthquakes in 17 lakes: implications for quantitative lacustrine palaeoseismology. Sedimentology 62, 1466–1496. https://doi.org/10.1111/sed.12193.
Vandekerkhove, Elke, Van Daele, Maarten, Praet, Nore, Cnudde, Veerle, Haeussler, Peter, De Batist, Marc, 2020. Flood-triggered versus earthquake-triggered turbidites: A sedimentological study in clastic lake sediments (Eklutna Lake, Alaska). Sedimentology. https://doi.org/10.1111/sed.12646.
Waldmann, N., Ariztegui, D., Anselmetti, F.S., Austin, J.A., Dunbar, R., Moy, C.M., Recasens, C., 2008. Seismic stratigraphy of Lago Fagnano sediments (Tierra del Fuego, Argentina) - a potential archive of paleoclimatic change and tectonic activity since the Late Glacial. Geol. Acta 6, 101–110. https://doi.org/10.1344/105.000000244.
Wilhelm, B., Nomade, J., Crouzet, C., Litty, C., Sabatier, P., Belle, S., Rolland, Y., Revel, M., Courboulex, F., Arnaud, F., Anselmetti, F.S., 2016. Quantified sensitivity of small lake sediments to record historic earthquakes: implications for paleoseismology. J. Geophys. Res. Earth Surf. 121, 2–16. https://doi.org/10.1002/2015JF003644.
Wils, K., Van Daele, M., Kissel, C., Moernaut, J., Schmidt, S., Siani, G., Lastras, G., 2020. Seismo-turbidites in Aysén Fjord (southern Chile) reveal a complex pattern of rupture Modes along the 1960 megathrust earthquake segment. J. Geophys. Res. Solid Earth. https://doi.org/10.1029/2020JB019405.
Yokoyama, R., Shirasawa, M., Pike, R.J., 2002. Visualizing topography by openness A new application of image processing to DEMs. Photogramm. Eng. Rem. Sens. 68, 257–265.
ZAMG, 2021. AEC - Austrian Earthquake Catalogue. Austrian Earthquake Catalogue. Computer file. Seismological Service of the Zentralanstalt für Meteorologie und Geodynamik (ZAMG) (Vienna, Austria).
Zolitschka, B., Francus, P., Ojala, A.E.K., Schimmelmann, A., 2015. Varves in lake sediments - a review. Quat. Sci. Rev. 117, 1–41. https://doi.org/10.1016/j.quascirev.2015.03.019.